Nanoscale

MINIREVIEW

Check for updates

Stimuli-responsive nanoparticle self-assembly at complex fluid interfaces: a new insight into dynamic surface chemistry

Jieun Heo, [ID] [a] Seunghwan Seo, [ID] [a] Hongseok Yun [ID] *[b] and Kang Hee Ku [ID] *[a]

The self-assembly of core/shell nanoparticles (NPs) at fluid interfaces is a rapidly evolving area with tremendous potential in various fields, including biomedicine, display devices, catalysts, and sensors. This review provides an in-depth exploration of the current state-of-the-art in the programmed design of stimuli-responsive NP assemblies, with a specific focus on inorganic core/organic shell NPs below 100 nm for their responsive adsorption properties at fluid and polymer interfaces. The interface properties, such as ligands, charge, and surface chemistry, play a significant role in dictating the forces and energies governing both NP–NP and NP–hosting matrix interactions. We highlight the fundamental principles governing the reversible surface chemistry of NPs and present detailed experimental examples in the following three key aspects of stimuli-responsive NP assembly: (i) stimuli-driven assembly of NPs at the air/liquid interface, (ii) reversible NP assembly at the liquid/liquid interface, including films and Pickering emulsions, and (iii) hybrid NP assemblies at the polymer/polymer and polymer/water interfaces that exhibit stimuli-responsive behaviors. Finally, we address current challenges in existing approaches and offer a new perspective on the advances in this field.

[a]*School of Energy and Chemical Engineering, Ulsan National Institute of Science and Technology (UNIST), Ulsan 44919, Republic of Korea. E-mail: kangheeku@unist.ac.kr*
[b]*Department of Chemistry and Research Institute for Convergence of Basic Science, Hanyang University, Seoul 04763, Republic of Korea. E-mail: yunhs@hanyang.ac.kr*

1. Introduction

The self-assembly of core/shell nanoparticles (NPs) at a fluid interface represents a captivating realm within the field of nanotechnology, offering numerous opportunities for the design and creation of functional materials with tailored properties.[1–3] For example, the high mobility of NPs at fluid interfaces enables rapid self-assembly or directed assembly

Jieun Heo received her B.S. in Energy Engineering at the Ulsan National Institute of Science and Technology (UNIST). She is pursuing a combined MS/Ph.D. program in the School of Energy and Chemical Engineering at UNIST, guided by Prof. Kang Hee Ku. With an interest in the field of colloid interface engineering, her academic pursuits are centered on nanoparticle assembly at fluid interfaces, aiming to fabricate thin films that can be utilized in batteries, catalysts, and sensors.

Jieun Heo

Seung Hwan Seo is currently serving as a master under the guidance of Prof. Kang Hee Ku in the School of Energy and Chemical Engineering at UNIST. He graduated from the Department of Chemical Engineering and Applied Chemistry at Chungnam National University in 2023. His research focuses on nanoparticle self-assembly at air/liquid and liquid/liquid interfaces and their transfer to solids. He aims to devise a simple method for creating nanoparticle thin films, with potential applications in electrodes and catalysts.

Seunghwan Seo

into two- or three-dimensional colloidal arrays with unique optical, magnetic, or electronic properties.[4–6] When NPs attach to an interface, they lower the Gibbs free energy, which depends on the square of the particle's radius, thereby stabilizing the overall system.[7] These NPs can selectively attach to or detach from the interface if the energy supplied is enough to overcome certain thermodynamic barriers. This process allows for a dynamic rearrangement of the NPs at the interface.[8] Therefore, a soft and adaptable fluid interface is key to effectively positioning NPs in a dynamic way. Particularly fascinating in this area of study is how NPs organize themselves in response to different triggers, such as temperature shifts, pH changes, light exposure, or external fields. The intricate interplay between various colloidal interactions (*e.g.*, van der Waals force, electrostatic interactions, and capillary force) influences the NP assemblies at the fluid interface and their functionalities.[9–11] The stimuli-responsiveness of NP arrays is attributed to the characteristics of either the organic ligands adsorbed on NP surfaces or the inorganic cores of the NPs.[12,13] Achieving neutral wetting conditions for different fluids at the NP interface is crucial for ensuring the long-term stability of the NP array, although it can be a complex task. In this context, there is a growing interest in designing ligand materials that facilitate fluid–NP interactions.[14–16] These ligands are typically organic molecules, polymers, and oligomers, covalently linked to the surface of NPs.[17] The key to achieving the responsive assembly and disassembly of NPs is dynamic reversibility in the intermolecular interactions between the fluid and organic materials that serve as ligands through external stimuli.

Over the decades, numerous reviews covering theoretical and experimental studies of the self-assembly of NPs at liquid/liquid or liquid/air interface have been published.[18–22] The majority of these reviews have primarily emphasized the thermodynamic interpretation of the core–shell structures that achieve static equilibrium for NP adsorption. However, the significance of designing organic ligands, particularly in accordance with the physical principles that govern the dynamic NP interactions, has been relatively unexplored in achieving responsive NP arrays. This review aims to present the current state-of-the-art in the programmed design of stimuli-responsive NP assemblies. We narrow our scope to inorganic core/organic shell NPs with sizes below a few tens of nanometers for two main reasons. First, these NPs have a lower adsorption barrier and are more responsive to external stimuli compared to larger particles, while their surface properties can be finely tuned through organic ligands.[23] Second, their size aligns well with the domain size in polymer/NP hybrid systems, typically in the tens of nanometers range, ensuring compatibility and effective interaction.[24,25] These two factors together enable the NPs to assemble responsively at interfaces, even in a reversible manner. Our primary emphasis is on elucidating the principles that govern the surface chemistry of NPs in a reversible manner, followed by detailed experimental examples. The stimuli-responsive NP assembly covered in this review comprises four key aspects: (i) stimuli-triggered assembly at the air/liquid interface; (ii) dynamic behavior at the liquid/liquid interface, encompassing films and Pickering emulsions; hybrid NP assembly (iii) at the polymer/polymer interface and (iv) polymer/water interfaces that exhibit stimuli-responsive behaviors (Scheme 1). We introduce a new perspective on utilizing specific polymer interfaces in NP assemblies, exploring their similarities and differences with air/liquid and liquid/liquid interfaces. Furthermore, we will address emerging trends and challenges, and suggest future directions, with a strong emphasis on the importance of interdisciplinary collaboration and the need for innovative solutions.

Hongseok Yun

Hongseok Yun is an assistant professor in the department of chemistry at Hanyang University. He received his B.S. and M.S. degrees in chemistry from University of Chicago in 2010. He completed his Ph.D. research under the guidance of Prof. Christopher B. Murray from University of Pennsylvania in 2015. After the Ph.D. degree, he worked as a postdoctoral researcher in Prof. Bumjoon Kim's group at KAIST until 2020. His current research interests include the synthesis and self-assembly of inorganic nanoparticle–polymer hybrid materials for stimuli-responsive smart materials and energy storage/harvesting applications.

Kang Hee Ku

Kang Hee Ku is currently serving as an assistant professor in the School of Energy and Chemical Engineering at UNIST. She completed her doctorate in 2018 under the guidance of Prof. Bumjoon Kim at KAIST and then worked with Prof. Timothy Swager at MIT as a postdoctoral researcher until 2020. Her research focuses on understanding the physical and chemical behavior of soft matter based on polymer science and colloid interface engineering to apply them in real-word life. Her current interests lie in the development of bio-inspired photonic crystals and intelligent colloids for microdisplays, sensors, and photonic cosmetics.
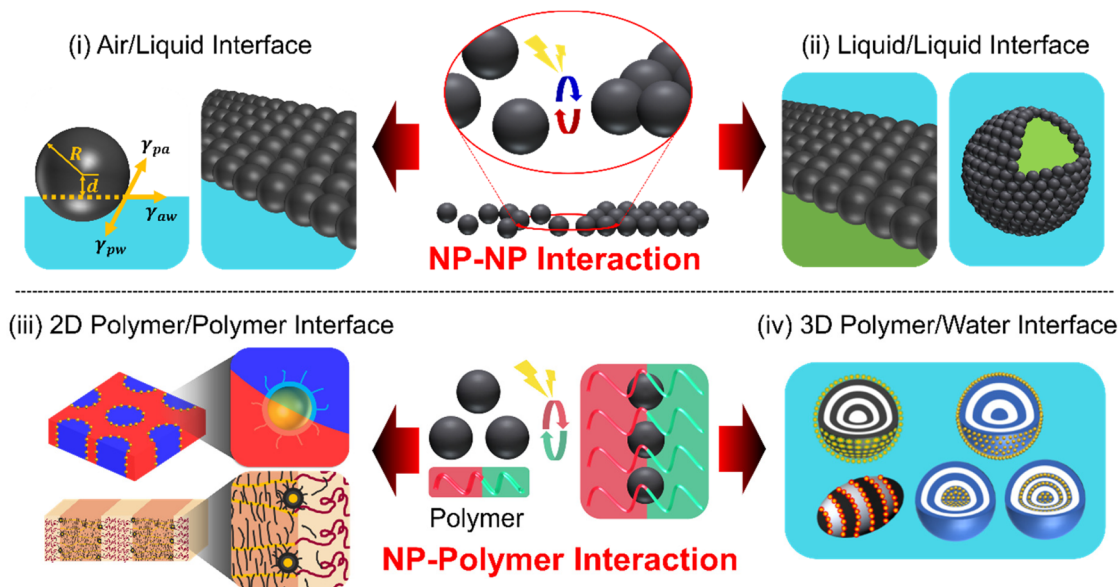
Scheme 1 Schematic illustration of stimuli-responsive self-assembly of NPs in complex fluids in this minireview: (i) NPs at air/liquid interface, (ii) NPs at liquid/liquid interface, (iii) NPs at polymer/polymer interface, and (iv) NPs at polymer/water interface.

2. Self-assembly mechanism: NPs at fluid interfaces

At soft air/liquid or liquid/liquid interfaces, NPs exhibit high mobility, allowing them to rapidly form dense assemblies. When NPs are trapped at a fluid interface, their assembly is primarily driven by the reduction of interfacial energy, as described by Gibbs free energy. To obtain an ordered NP array from a loose packing structure through external stimuli, it is essential to consider additional interactions that can influence the alignment of neighboring NPs.[7] In this context, we will briefly introduce the thermodynamic and kinetic approaches for NP assembly with particular emphasis on NP–NP interactions triggered by external stimuli.

2.1. Thermodynamic and kinetic approaches

When spherical particles with a radius r are present at the interface between adjacent α and β fluid phases, they occupy an area equivalent to the interfacial area. The adsorption of particles at the interface reduces Gibbs free energy, expressed by the following equation:

$$\Delta E = -\pi r^2 \gamma_{\alpha\beta}(1 \ \pm \ \cos\theta)^2$$

here, θ represents the contact angle, and $\gamma_{\alpha\beta}$ is the interfacial tension between the α and β fluids.[26] The favorable interfacial adsorption of particles is due to the consistently negative Gibbs free energy. The stability of particles at the interface is influenced by thermodynamic factors, including particle size, shape, and wettability.[9] The size of the Gibbs free energy is proportional to the square of the radius of the particle. Typically, particles larger than 10 nm tend to form nearly irreversible assemblies due to substantial thermal energy

barriers.[27–30] However, some studies show that sub-100 nm nanoparticles, which have adjustable wettability through ligand design and are responsive to external stimuli, can display dynamic behavior at fluid interfaces.[31–33] This phenomenon is attributed to that either their wettability is highly conducive to interacting with a specific fluid,[23] or the interactions between particles are modified due to external stimuli, consequently reducing the thermal energy barrier.[34] Additionally, kinetics, particularly the mass transfer of volatile liquids, plays a pivotal role in organizing NPs at the interface.[35–37] Typically, a faster response in stimuli-responsive NP assembly is observed at higher temperatures and lower potential barriers.[38]

2.2. Stimuli-responsive NP interaction

Besides the decrease in interface energy achieved by NP adsorption, forming an ordered NP array requires specific interactions that can counterbalance the entropy penalty associated with NP assembly. The dominant interactions between a pair of NPs are van der Waals and electrostatic interactions as described in the Derjaguin–Landau–Verwey–Overbeek theory.[39] van der Waals interactions typically result in attraction between similar particles within the same medium,[40] and when this attraction exceeds electrostatic repulsion, it promotes the self-assembly of NPs. Therefore, external stimuli capable of modulating or overcoming electrostatic repulsion are crucial for forming well-aligned NP arrays. The organic ligand design plays a key role in controlling NP interactions, including their responsiveness to external stimuli and wettability. Fig. 1 summarizes the NP interactions induced by chemical (*e.g.*, pH) and physical (*e.g.*, light, temperature, and electromagnetic fields) stimuli.[41]
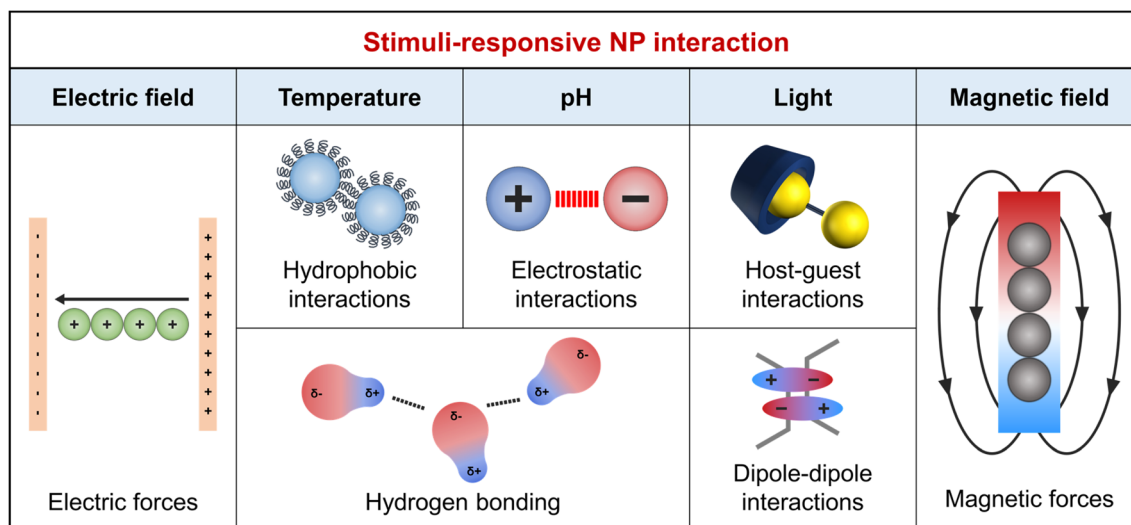
Fig. 1 Summary of the external stimuli and corresponding physical interactions to induce self-assembly of NPs at fluid interface.

Chemical stimuli, such as changes in pH due to acid, base, or CO_2 addition, adjust the surface charge of organic ligands. For instance, the addition of a base increases the pH, leading to increased electrostatic repulsion between acidic functional groups like COOH and enhanced NP dispersion in solvents. Conversely, low pH weakens this repulsion and enhances van der Waals forces, promoting NP assembly.[42] Additionally, pH affects hydrogen bond strength, varying with the density of surface anchoring groups (*i.e.*, –OH, –COOH, or $-NH_2$).[43] Physical stimuli include light, temperature, and electromagnetic fields. Light-responsive groups, such as nitrobenzyl and coumarin esters, break down into smaller segments upon light absorption.[44] Photoisomerizable groups, such as azobenzene, undergo structural transformations under specific light wavelengths, affecting molecular volume and hydrophilicity, crucial for NP wetting properties and host–guest chemistry.[45] Dipole–dipole interactions occur between molecules that have a permanent electric dipole moment. Alkanethiol ligands significantly increase the dipole moment of Au NPs. Furthermore, the introduction of azobenzene to these ligands allows for interaction switching under different light wavelengths through photoisomerization. UV light activates these interactions, while visible light deactivates them.[46] These enhanced attractive forces overcome the electrostatic repulsion between NPs, facilitating the attachment of adjacent particles[47] and thereby enabling the photo-responsive assembly of NPs.[48] Photo-initiators, such as acrylate-based ligands, induce the conversion of monomers into a polymer upon exposure to specific wavelengths of light.[49] Hydrogen bonds, essential in host–guest chemistry, exhibit temperature sensitivity. Higher temperatures break hydrogen bonds due to increased kinetic energy, altering molecular structures. Lower temperatures favor hydrogen bond reformation.[50] This behavior is key for thermoresponsive polymer ligands on NPs, affecting solubility and surface interactions. Notably, around specific temperature
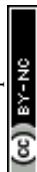
thresholds, such as the lower critical solution temperature (LCST), these polymers lose hydrogen bonds with water molecules and become hydrophobic, promoting clustering and reducing interaction with polar solvents.[51] In external electric fields, the polarization of ligands causes their reorientation, affecting NP arrangement. Magnetic NPs align and magnetize in magnetic fields, enabling directional alignment.[52]

3. NP arrays at fluid interfaces

3.1. Self-assembly of NPs at an air/liquid interface

For the air/liquid interface system, the physicochemical stimuli can be directly applied, taking advantage of the direct contact with the air interface. In some cases, when NPs are assembled at the air/water interface, they form loosely packed structures, requiring additional effort to create a more organized array. The conventional interfacial tension gradient method employs volatile liquids such as ethanol and ethyl acetate to achieve a well-ordered NP array by reducing interfacial energy.[53,54] The method involves using volatile liquids with different surface tensions to create a capillary force, pulling NPs towards higher surface tension regions. Careful control of solvent addition allows manipulation of these forces, compressing interparticle distance and facilitating self-assembly into a well-ordered array. Alternatively, specific external stimuli can replace volatile liquids, when these stimuli can trigger the manipulation of the interparticle distance between NPs. In this section, we present recent experimental progress in stimuli-triggered NP assembly at an air/liquid interface.

3.1.1. Light-responsive assembly. While thiol groups are commonly employed for modifying NP surfaces, the utilization of photoisomerizable ligands has faced challenges in achieving uniform NP arrays at air/liquid interface. The design hurdle involves achieving substantial alterations in the inter-

facial tension gradient or NP–NP interactions for sub-100 nm NPs segregated at the air/liquid interface.[55] Consequently, the adoption of irreversible photo-responsive assembly principles, such as photopolymerization and photocleavage, has emerged as a prominent strategy to achieve light-responsive NP assembly. For instance, the Chen group successfully achieved densely packed arrangements of Au NPs modified with acrylamide through UV-triggered polymerization (Fig. 2(a)). Under UV irradiation, the cross-linking of adjacent functional groups on the surface of Au NPs enabled the formation of a uniform film through the reduction of porosity.[31] Demonstrating the application of photocleavage to induce the transformation of loosely assembled NPs into a condensed structure, the Leggett group reported the method of photo-oxidation of the UV-light-induced alkanethiol group.[56] This technique, initially developed for site-specific patterning, was later applied by the Kawai group to induce the formation of metal nanosheets through the breakdown of NP ligands. Subjecting dodecanethiol-functionalized Au NPs under 248 nm light, they triggered ligand decomposition at the air/water interface, resulting

in the fusion of Au NPs into a nanowire structure due to the energetic instability.[57] The synthesis of Ag nanosheets was also explored by the same group, employing anionic Ag NPs and a cationic surfactant, dioctadecyl dimethylammonium chloride (DODAC). UV irradiation induced a morphological change in the Ag NP monolayer, leading to the formation of nanosheets with a mesh-type structure. The photocleavage of DODAC played a crucial role in this process, lowering the surface pressure and promoting fusion between adjacent Ag NPs. UV further activates Ag NPs to form Ag nanosheets.[58] These advancements in metal NP synthesis and nanowire structure assembly hold promise for the development of conductive films.

3.1.2. Temperature-responsive assembly. The Paczesny group introduced a poly(N-isopropyl acrylamide) (PNIPAM) capping layer into NPs to implement temperature-responsive NP assembly at the air/liquid interface. When the PNIPAM ligands were attached to the surface of the Fe_xO_y@SiO_2 NPs, a uniform 2D film was obtained at a high temperature of 40–42 °C, above the LCST of the PNIPAM. In contrast, below
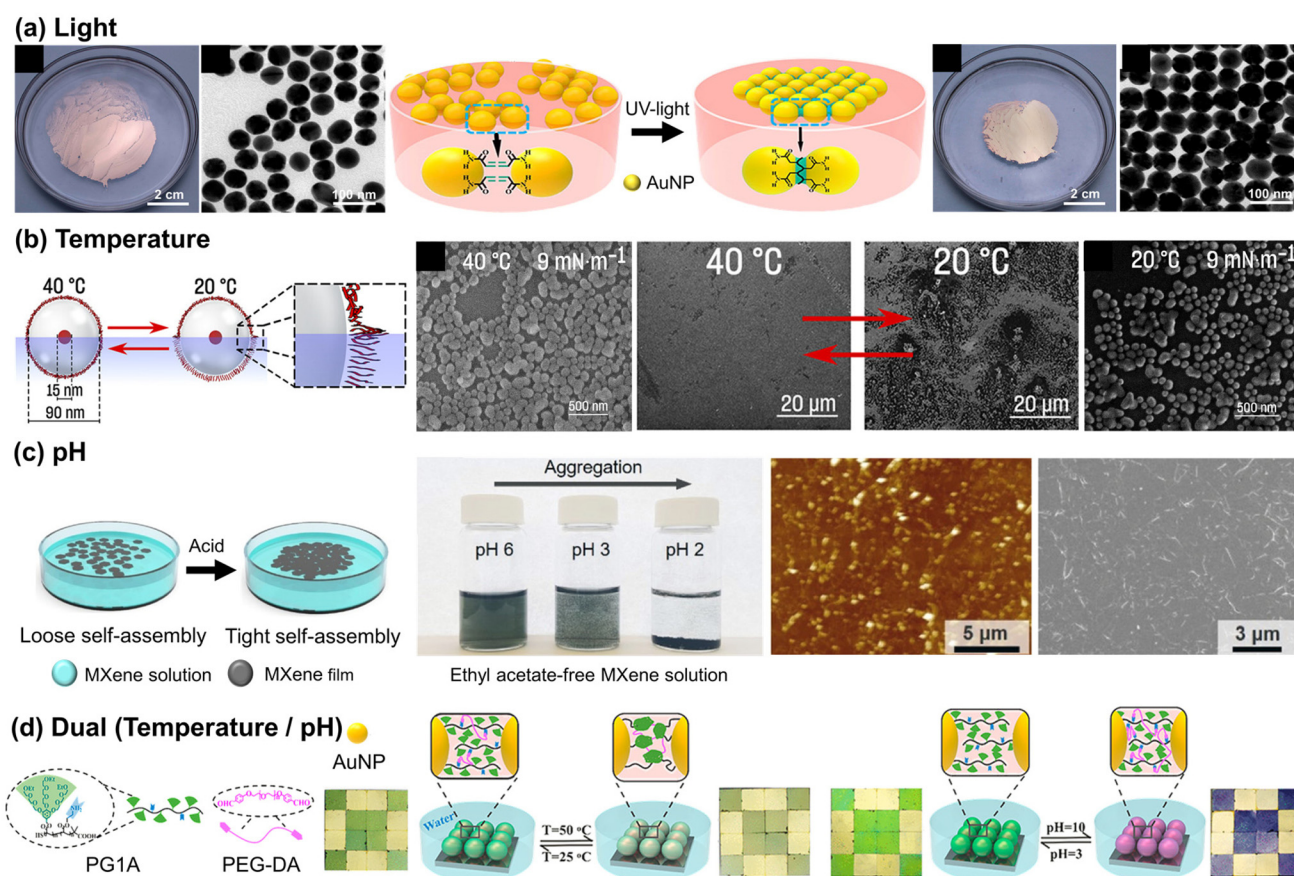

Fig. 2 Stimuli-responsive self-assembly of NP at air/liquid interface: (a) assembly of the Au NP monolayer film by UV-induced interfacial cross-linking at the air/water interface. Reproduced from ref. 31 with permission from American Chemical Society 2018; (b) temperature-responsive assembly of NPs decorated with PNIPAM. Reproduced from ref. 32 with permission American Chemical Society 2023; (c) pH-responsive arrangement of the MXene film between loose and dense packing structures. Reproduced from ref. 37 with permission from Wiley 2022; (d) temperature- and pH-dual responsive NP array with an oligoethylene-glycol-based dendronized copolymer (PG1A) and polyethylene glycol dibenzyl aldehyde (PEG-DA). Reproduced from ref. 64 with permission American Chemical Society 2018.

the LCST of PNIPAM, specifically at 18–20 °C, the film caused aggregates attributed to the extended and coiled conformations of PNIPAM chains (Fig. 2(b)).[32]

Another effective approach for temperature adjustment is the photothermal method, wherein light irradiation increases temperature near NPs through the conversion of absorbed photons into heat energy (phonons), thereby facilitating the thermally-driven assembly of NPs. As an example, the Deng group achieved reversible assembly of Au NPs by using light-induced thermal evaporation of liquid. This method, based on the manipulation of surface tension gradients, allows efficient control over NP assembly without affecting surface charge or ligand molecule structure. During the synthesis of oleylamine-coated Au NPs, some of the oleylamine molecules on the Au NPs were oxidized into carbonyl groups, allowing hydrogen bonds with the remaining unoxidized oleylamine groups.[59] The presence of an excess amount of oleylamine in the chloroform solution of Au NPs led to the formation of oleylamine double layers. This occurred through the hydrogen bonding between the excess oleylamine and the grafted oleylamine on the surface of Au NPs, stabilizing the Au NP dispersion and thus preventing the self-assembly of Au NPs. In the absence of excess oleylamine or with the replacement of surface ligands by n-hexadecane thiol, the NPs were assembled through photothermal-driven evaporation of chloroform. The reversible assembly behavior was governed by the metastable state, with films coated with both oleylamine and alkyl thiol groups exhibiting negative thermodynamic potential energy changes. In this state, the film can be easily disassembled by an external force and subsequently reassembled through a light-irradiation plasmonic effect.[60] In a similar way, the Pillai group reported a method by utilizing DMSO hygroscopicity and sunlight-driven water evaporation as driving forces. Thymine thiol-functionalized Au NPs dispersed in DMSO formed stable 2D assemblies due to moisture absorption, while photothermal-induced temperature increase to 80 °C resulted in disassembly of the NPs through water evaporation.[61]

3.1.3.   pH-Responsive assembly. As demonstrated in the previous section, since pH adjustment modifies the surface charge, it is useful to leverage the van der Waals interaction and electrostatic interaction. High pH leads to large electrostatic repulsions, whereas low pH decreases electrostatic repulsion, thereby facilitating NP assembly. The Ahn group demonstrated a tightly assembled MXene film by adding hydrochloric acid to a loosely assembled Ti_3C_2 MXene film (Fig. 2(c)). As-synthesized MXene flakes exhibited a zeta potential of less than −40 mV at pH 6.0, causing strong electrostatic repulsion. Typically, the zeta potential of above −30 mV is necessary to reduce electrostatic repulsion and to increase the adherence of interflake contacts. By reducing the pH to 3 by adding drops of hydrochloride, they found that the zeta potential of the MXene flakes increased to −30 mV, inducing aggregation of the MXene flakes. This pH-driven assembly of the Ti_3C_2 MXene led to the formation of a film with low electrical resistance and high stability.[37] The pH-responsive polymers also can be intro-

duced to provide pH-responsiveness for NPs. For example, when Au NPs were capped with alkyl thiol-terminated poly (acrylic acid) (PAA), the carboxyl group underwent protonation below pH 3, leading to the creation of hydrogen bonds between NPs and adjacent molecules. Consequently, the hydrophobic alkyl chains became dominant, prompting the NPs to migrate to the interface to minimize their contact with water. The presence of the dihexadecanoyl-3-trimethyl-ammonium-propane played a pivotal role by attracting PAA-functionalized Au NPs, contributing significantly to their interface assembly process due to its positively charged head groups that attract the negatively charged carboxyl groups of PAA through electrostatic interactions. Lowering the pH enhanced these electrostatic attractions and also promoted hydrophobic interactions between the hydrocarbons as well as hydrogen bonding between NPs, leading to a more ordered assembly.[62]

3.1.4.   Dual-responsive assembly. A dual-responsive ligand system for NPs has recently been applied in NP arrays at air/liquid interfaces. The Chen group employed a temperature- and pH-sensitive ligand, trithiocarbonate-terminated oligo (ethylene glycol)-based dendronized copolymer, to provide dual-responsiveness for Au NPs. In the water/hexane system, ethanol reduces surface charge similarly to the thiol group because it is competitively adsorbed on the NP surface, as demonstrated by the Vanmaekelbergh group.[63] Subsequently, polyethylene glycol dibenzyl aldehyde was introduced, creating a polymer network. Evaporation of hexane led to the formation of a monolayer film of Au NPs at the air/water interface. When the temperature increased from 25 to 50 °C, the polymer network was broken and clumped together, reducing the interparticle distance. Simultaneously, a pH decrease from 10.0 to 3.0 caused the imine bond to break, increasing the distance between NPs at the air/water interface. These two orthogonal responsive behaviors were reversible and demonstrated the ability to evoke color changes in NPs.[64]

3.2.   Self-assembly of NPs at a liquid/liquid interface

Self-assembly of NPs at liquid/liquid interface has proven to be a cheap, convenient, and efficient route to obtain densely packed layers of NPs with minimal interparticle distances. When NPs assemble at the liquid/liquid interface, they can form either a two-dimensional monolayer film or a three-dimensional structure, called Pickering emulsions.[65–69]

3.2.1.   Two-dimensional assembly into a monolayer film. First, we will discuss how changes in the interaction of organic ligands of NPs, induced by light, redox reactions, or electric fields, can facilitate the formation of the NP monolayer film by achieving a dynamic equilibrium state. In a recent study by the Russell group, a photo-switchable jamming-to-unjamming transition of Au NPs at the oil/water interface was demonstrated. This transition was achieved by exploiting the host–guest interaction between α-cyclodextrin (α-CD) ligands on the NPs and azo-terminated poly-L-lactide (Azo-PLLA), as illustrated in Fig. 3(a). Azo-PLLA in toluene forms hydrogen bonds with the hydroxyl group of α-CD ligands on the AU NPs in
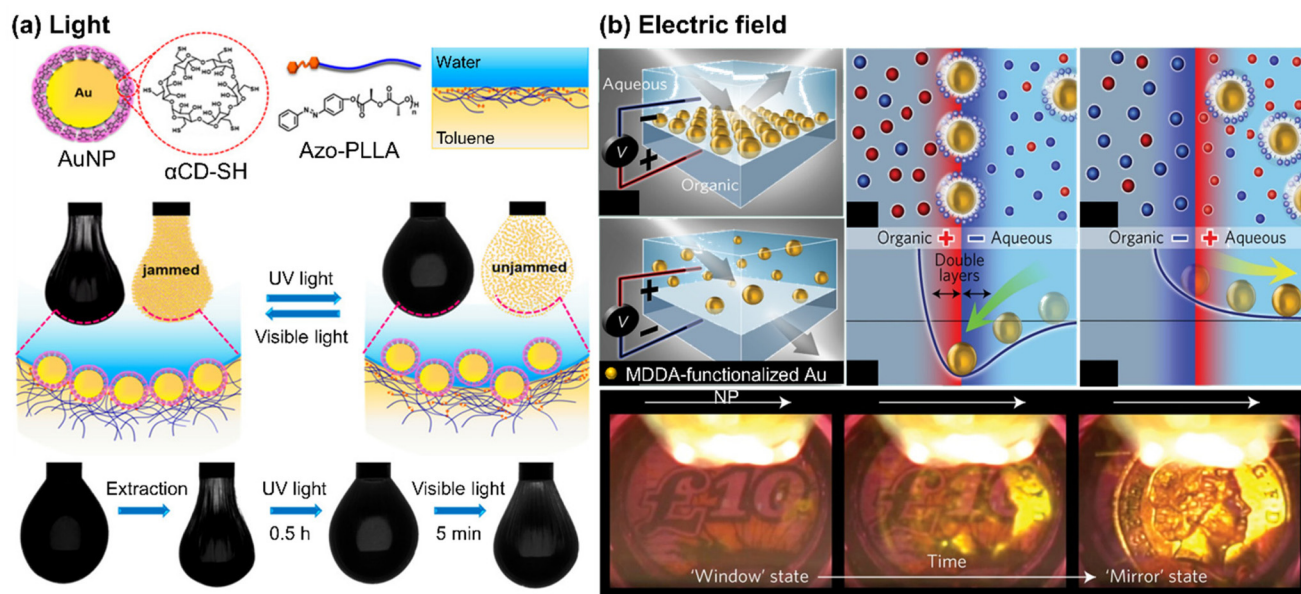
Fig. 3 Stimuli-responsive self-assembly of NPs at liquid/liquid interface to form a monolayer film: (a) photo-switchable jamming-to-unjamming transition of Au NPs at oil/water interface, driven by host–guest molecular recognition. Reproduced from ref. 70 with permission from American Chemical Society 2020; (b) reversible electro-tunable liquid mirror based on voltage-controlled self-assembly/disassembly of plasmonic NPs at the interface between two immiscible electrolyte solutions. Reproduced from ref. 74 with permission from Nature Publishing Group 2017.

water, promoting toluene/water interfacial assembly. When exposed to visible light, Azo-PLLA underwent isomerization from *cis* to *trans* configuration, enhancing host–guest molecular recognition and resulting in the dense assembly of the NPs. On the other hand, under UV irradiation, Azo-PLLA transitioned back to its *cis* form, causing the NPs to disengage from the α-CD pocket. Thus, the NP layer became loosely packed due to reduced interaction with the Azo-PLLA.[70] They also reported a similar system involving the redox-responsive reversible assembly of Au NP through molecular recognition of β-cyclodextrin (β-CD) and ferrocene (Fc). When Fc-PLLA was oxidized, the Fc group converted to the Fc^+ and lost affinity with β-CD, leading to an increase in interfacial tension in toluene. As a result, β-CD-functionalized Au NPs were removed from the interface between the liquid and Fc-PLLA.[71]

When the organic ligand of NPs carries a surface charge, it becomes possible to control the assembly of these NPs using an external electric field.[72] For example, in one approach, the positively charged trimethylammonium-terminated Au NPs were utilized to facilitate their transport from the aqueous phase to the organic phase in two immiscible electrolyte solutions when subjected to an electric field. By adjusting the voltage, a dense array of NPs was achieved.[73] Kornyshev and co-workers developed a voltage-controlled liquid mirror by assembling negatively charged Au NPs, functionalized with 12-mercapto dodecanoic acid (MDDA). As depicted in Fig. 3(b), the Au NPs were effectively adsorbed or desorbed at the interface, depending on the direction of the electric field. Applying a positive voltage to the aqueous solution dispersed the NPs, while a negative voltage led to the NPs being most stably located at the interface with the organic electrolyte.[74]

To facilitate denser arrangements of NPs, it is essential to diminish electrostatic repulsion. A prevalent approach to overcome this challenge involves the binding of electrically neutral organic ligands to the NP surface. Notably, the modification of NPs with a metal core using charge-neutral thiols is a conventional method for generating NP monolayers at the liquid/liquid interface. For example, by reducing the surface charge of hydrophilic Au NPs through acetone introduction and subsequent agitation, thiolates replaced citrate anions as ligands.[75,76] This allowed for the creation of ordered arrays of Au NPs with neutral ligands, mitigating electrostatic repulsion. At the hexane/water interface, these NPs assembled into a densely packed monolayer film.[77] In a similar manner, perfluorodecanethiol (PFT) was introduced as an *in situ* NP surfactant. Initially, Au NPs were dispersed in water, and hexane with PFT was added. By increasing the PFT content, they enhanced the hydrophobicity of the NPs, thereby reducing the kinetic energy barrier associated with interface assembly.[78,79]

3.2.2. Three-dimensional assembly into Pickering emulsions. Pickering emulsions are stabilized through the adsorption of solid particles, which are transported to the liquid/liquid interface by mechanical stirring or convection. There is a growing interest in developing Pickering emulsions that exhibit responsiveness to external stimuli, enabling phase inversion or emulsification/demulsification. As previously discussed, NPs larger than 100 nm tend to adsorb irreversibly at interfaces due to thermodynamic preferences, resulting in limited examples of responsive Pickering emulsions stabilized by organic/inorganic composite particles over 100 nm.[80,81] For sub-100 nm NPs, recent advances in stimuli-responsive Pickering emulsions often entail the introduction of ionizable

View Article Online

Nanoscale

surfactant molecules to provide NPs with responsive surface charges. Unlike air/liquid interfaces, light is not utilized as a stimulus due to the potential interference caused by the emulsion's turbidity, making light-mediated systems less efficient. Instead, temperature and pH variations are commonly employed as stimuli for Pickering emulsions.

Ding and colleagues demonstrated a thermo-sensitive Pickering emulsion stabilized by hydrophilic silica NPs and poly(ethylene oxide-*block*-propylene oxide-*block*-ethylene oxide) (PEO-*b*-PPO-*b*-PEO) (Fig. 4(a)). At room temperature, stable paraffin oil-in-water Pickering emulsions were obtained using the silica NPs with surface-adsorbed PEO-*b*-PPO-*b*-PEO through hydrogen bonds. Upon heating to 55 °C, phase separation occurred due to disruption of the hydrogen bond between the PEO and the silanol group on the silica NP. Subsequent cooling and homogenization allowed for the polymer re-adsorption onto the silica surface through hydrogen bond formation, enabling the re-emulsification of the Pickering emulsion. The length of the PEO group capable of forming hydrogen bonds with silanol groups played a critical role in determining the temperature tolerance of the Pickering emulsion.[82] Similarly, the Palmqvist group modified the surface of silica NP by combining hydrophilic methyl poly (ethylene) glycol (mPEG) and hydrophobic propyl groups to attain reversible phase inversion between oil-in-water and water-in-oil configurations. Salt concentration, pH, and heat were the crucial factors that influenced phase inversion. Temperature changes can cause phase inversion in emulsions stabilized by nonionic PEG-based surfactants. This happens due to the conformational changes in the polyoxyethylene chains. At lower temperatures, polar conformations dominate, but as temperature increases, nonpolar conformations prevail, leading to a phase inversion from oil-in-water to water-in-oil at the phase inversion temperature. Lowering pH facilitated the adsorption of the PEG chain onto the silica, reducing electrostatic repulsion, whereas an increased salt concentration caused interfacial NP adsorption, both of which consequently decreased the temperature required for the phase inversion.[83]

Typically, pH-responsive Pickering emulsions are stimulated by either acid/base addition or CO_2 bubbling. Acid–base addition strategies involve the carboxylate group either on the NP surface or within the surfactant molecules. The Cui group presented a Pickering emulsion employing positively charged alumina NPs and sodium carboxylate-derived selenium surfactants as illustrated in Fig. 4(b). The carboxylic sodium groups in the surfactant could be anionic or nonionic based on pH levels. At a high pH (around 10.29), the anionic carboxylate surfactant and alumina NPs worked together to stabilize the Pickering emulsion. However, lowering the pH led to the protonation of carboxylate surfactants, transforming them into nonionic carboxylic acid. This change reduced the electrostatic attraction between the NPs and the surfactants, consequently destabilizing the Pickering emulsions.[84] Furthermore, they also used zwitterionic carboxyl betaine surfactants and negatively charged silica NPs to create pH-responsive Pickering emulsions. These emulsions remained stable only at a pH of 5
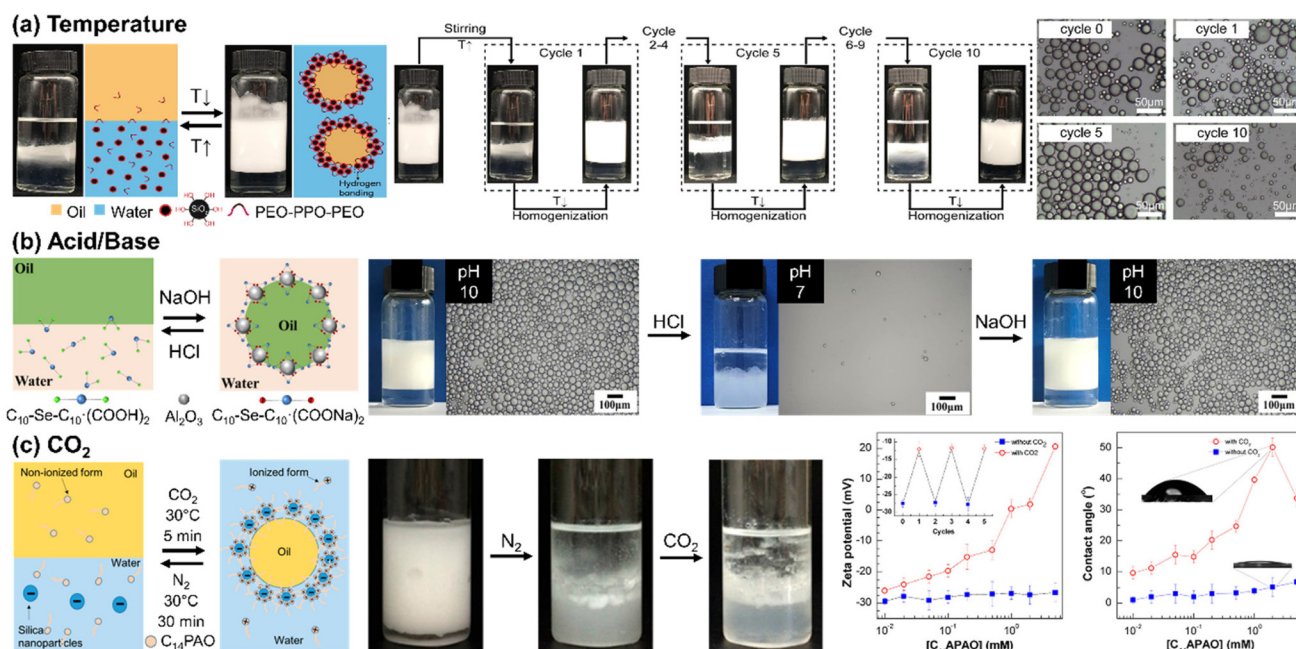

Fig. 4 Stimuli-responsive self-assembly of NPs at liquid/liquid interface to form Pickering emulsions. (a) Temperature-responsive emulsification and demulsification of Pickering emulsion droplets stabilized by silica NPs modified by PEO-*b*-PPO-*b*-PEO. Reproduced from ref. 82 with permission from Elsevier 2022; (b) pH-induced Pickering emulsion stabilized by alumina NPs and sodium carboxylate-derived selenium surfactant. Reproduced from ref. 84 with permission from American Chemical Society 2021; (c) CO_2-switchable emulsification and demulsification of Pickering emulsions. Reproduced from ref. 86 with permission from American Chemical Society 2018.

or lower, as this pH range facilitated electrostatic attraction between the negatively charged NPs and the positively charged carboxyl betaine surfactants.[85]

When CO_2 is used to trigger pH variation, no hazardous byproducts are produced, thus reversible CO_2-induced Pickering emulsions have the advantages of biocompatibility and reuse. The Fang group reported myristylamidopropyl amine oxide ($C_{14}PAO$), a CO_2-responsive surfactant that can switch between cation and non-ion forms reversibly, as summarized in Fig. 4(c). The highly polar head group of $C_{14}PAO$ allows for a transition between nonionic and cationic states in response to pH changes. Therefore, a CO_2-driven increase in pH led to the conversion of $C_{14}PAO$ to $C_{14}PAOH^+$, which was effectively adsorbed onto negatively charged silica NPs through electrostatic attraction. Consequently, by CO_2 bubbling, the $C_{14}PAOH^+$-functionalized silica NPs formed stable Pickering emulsions, while demulsification occurred when N_2 bubbling removed the CO_2.[86] Wang and co-workers utilized negatively charged silica NPs and ionic liquids, N-alkylimidazole bicarbonates. CO_2 enables the formation of carbonic acid (H_2CO_3), which protonates N-alkylimidazole and converts to N-alkylimidazole bicarbonates. This molecule was ionized in an aqueous solution, and the N-alkylimidazole cations were adsorbed on the surface of the silica NPs to form Pickering emulsions.[87] In a similar manner, Jiang and colleagues employed surfactant ionization to enable adsorption and desorption on NPs. They utilized 11-(N,N-dimethylamino)sodium undecanoate (NCOONa), featuring both anion carboxylate and tertiary amine groups, to bind to positively charged alumina NPs through electrostatic forces, thereby stabilizing the emulsion.[88] This stability was reversed by CO_2 bubbling, which made the surfactant more hydrophilic, causing it to desorb from the NPs and move into the water phase, aiding in demulsification. The Cui group developed a biphasic biocatalyst system using a CO_2-responsive Pickering emulsion. They loaded the enzyme lipase, N,N-dimethyldocylamine, which was converted to ammonium bicarbonate by CO_2 bubbling. These cationic ammonium surfactants were adsorbable onto negatively charged silica NPs, thereby facilitating the process of Pickering emulsification. Triggered by N_2 bubbling, the demulsification process effectively separated the oil and water phases: the product was isolated in the oil phase, while the enzymes and NPs remained in the aqueous phase, facilitating their subsequent separation and recycling.[89]

3.3. Self-assembly of NPs at polymer interfaces

In Sections 3.1 and 3.2, we explored the assembly of NPs at fluid (i.e., liquid and air) interface systems. Advancing this discussion, we now turn our attention to the crucial role of polymer interfaces in facilitating and directing these assemblies. Polymer chains, depending on their fluidic nature, serve as flexible and dynamic scaffolds for NP assembly, mirroring the behavior observed at air/liquid and liquid/liquid interfaces. This flexibility, combined with the inherent capacity to precisely control the spatial arrangement of the constituents, significantly enhances the functionality of the resulting nano-

composites, including optical, electronic, magnetic, and catalytic properties.[90,91] It is noted that the integration of NPs into the polymer matrix results in entropy penalties due to the elongation and compression of the surrounding polymer chains. Consequently, there is an entropy-driven preference for NPs to localize at the interface rather than within the polymer chain matrix, a process analogous to their adsorption at both air/liquid and liquid/liquid interfaces.[92] Distinct from air or liquid interfaces, polymer matrices offer an added advantage: their susceptibility to external stimuli manipulation.[93] Controlling properties of air and liquid interfaces typically demands an environment where pressure and temperature are tightly regulated, a process often marred by inefficiency. By contrast, polymer matrices exhibit responsive behaviors such as swelling/deswelling in response to physicochemical stimuli or undergoing structural modifications when exposed to specific substances.[94,95] Moreover, polymer interfaces afford an exceptional degree of control over the positioning of NPs. This is achieved through meticulously calibrating the size ratio between the NP and the NP–hosting polymer domain, as well as fine-tuning the interactions between NP ligands and polymer chains. In this section, we categorize polymer interfaces into two distinct types: two-dimensional polymer/polymer interfaces and three-dimensional polymer/water interfaces.

3.3.1. Self-assembly mechanism: NPs at polymer interfaces.
To create these hybrid structures with desirable properties, precise control over the local distribution, orientation, and interparticle distance of NPs at the polymer interface is critical.[96,97] Block copolymers (BCPs) are versatile scaffolds to organize NPs into structured arrangements due to their spontaneous self-assembly, giving rise to ordered nanostructures through non-covalent interactions.[92,98] Their arrangement is determined by the interplay between the enthalpic contributions (ΔH), related to interactions between BCPs and NP ligands, and the entropic contributions (ΔS), which arise from NP size, shape, or BCP domain properties.[99–101] In overall, the change in free energy during NP incorporation at the polymer interface can be expressed as follows.

$$\Delta G = (\Delta H_{ligand-BCP}) - T(\Delta S_{con} + \Delta S_{trans})$$

$\Delta H_{ligand-BCP}$ accounts for various interactions, such as van der Waals forces, ionic interactions, dipole–dipole interactions, and hydrogen bonding.[102–105] Stronger interactions enhance the enthalpic contribution, promoting NP integration. Meanwhile, ΔS_{con} is linked to the conformational entropy of polymer chains when NPs are introduced at the BCP interface. ΔS_{trans} represents the translational entropy resulting from the NP arrangements. The dominance of ΔS_{con} depends on the strength of enthalpic interactions and the relative size of NPs with respect to the radius of gyration (R_g) of the BCP chains. Specifically, when enthalpic interactions are weak or when the size of NPs exceeds the R_g of the BCP, ΔS_{con} takes precedence as the primary factor.[97] To alleviate the entropy penalty resulting from the integration of NPs, expanding the domain size of

the BCP can be an effective strategy.[106,107] The balance of these thermodynamic terms is crucial for the successful spatial arrangement of NPs at the BCP interface.

In this section, we first discuss the experimental developments in crafting controlled NP arrays at the BCP interface. Specifically, we emphasize recent efforts to engineer the chemical structure of core/shell NPs to fine-tune BCP–NP interactions, thus establishing an innovative hybrid BCP/NP system through interfacial assembly of NPs at the BCP interface. We also highlight the design rules of stimuli-responsive assemblies for these hybrid BCP/NP systems, with specific attention to the surface chemistry of the NPs and their responsive interaction with the BCP domains. Furthermore, we will expand our insight into three-dimensional hybrid systems involving colloidal particles where emulsion droplets serve as flexible and dynamic templates for guiding the polymer assembly.

3.3.2. Self-assembly of NPs at polymer/polymer interfaces.
Leveraging the interplay of enthalpic interactions between NPs and BCPs and entropy loss of the chains wrapping the NPs, as demonstrated in Section 3.3.1, we now introduce recent experimental advancements in the fabrication of 2D film and bulk nanocomposites.

In the BCP-guided self-assembly of NPs, the key factors dictating their location can be classified based on surface selectivity, which pertains to enthalpic considerations, and NP size dependence, affecting entropic considerations.[101,108] In particular, NPs that possess a non-selective preference for both blocks can assemble at the interface due to favorable enthalpic interactions.[109,110] For instance, when PS-coated Au NPs were co-assembled with polystyrene-*block*-poly(2-vinyl pyridine) (PS-*b*-P2VP) BCPs, the NPs located either at PS/P2VP interface or selective BCP domain depending on the PS grafting density.

Specifically, when the NPs were partially shielded by PS ligand (<1.3 chains per nm^2), they located at the interface due to strong favorable interactions between the bare Au surface and the P2VP domain.[111] Similar behavior was observed when Au NPs were coated with a mixture of PS and P2VP, with the assembly outcome dictated by the ratio between the two components.[112]

Recent advancements involve modifying the NP surface with ligands that strongly interact with one of the polymer blocks, such as hydrogen bonding. For example, the Hawker group synthesized Au NPs with thiol-terminated BCP ligands, forming a polyisoprene (PI) inner shell, and a PS outer shell (Fig. 5(b)).[113] These core–shell Au NPs were located within the PS domain due to the hydrophobic interaction between the ligand and PS domain. In contrast, the hydroxylated core–shell Au NPs were segregated to the PS/P2VP interface due to hydrogen bonding between the hydroxylated inner shell and the P2VP. Precise control over the number of hydroxyl groups enabled fine-tuning of the segregation behavior of the Au NPs.[114] Also, they investigated the interplay between core–shell Au–Pt NPs coated with the same BCP ligands and PS-*b*-P2VP. The Pt-shell was formed through the cross-linking of the PI brush of ligand in the presence of Pt catalyst. Prior to the cross-linking process, the NPs resided within the PS domain, primarily due to the enthalpic interaction between the outer PS brush of the ligand and the PS domain. However, following the cross-linking, NPs were located at the PS/P2VP interface due to the increased interaction between the P2VP domain and the residual Pt catalyst in the PI inner shell, particularly due to the reduced effective areal chain density of the PS brush on the PI shell compared to that on the NP surface.[115]
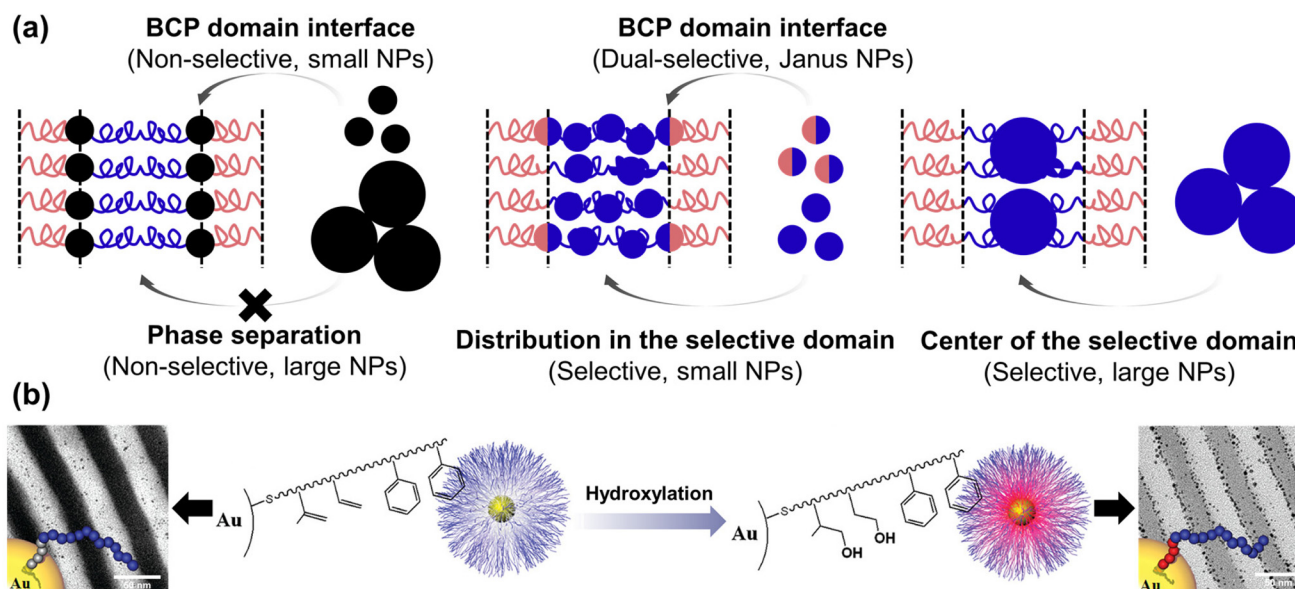

Fig. 5 BCP-guided self-assembly of NPs at the BCP interface. (a) Schematics for the selective localization of NPs within the BCP domains or at the BCP interface. Reproduced from ref. 101 with permission from Elsevier 2014; (b) controlled supramolecular assembly of core−shell Au NPs in PS-*b*-P2VP by hydrogen bonding. Reproduced from ref. 113 with permission from American Chemical Society 2011.

To achieve responsive transformation of NP assembly at the BCP interface, the enthalpic interactions between BCPs and NPs should be tunable in response to stimuli, either through responsive NP ligands or the polymer matrix, or both. The Watkins group employed UV-responsive ligands, poly(styrene)-*block*-poly(*o*-nitrobenzene acrylate) (PS-*b*-PNBA), for Au NPs to control the selectivity of the NPs towards different blocks of BCPs.[116] Initially, the ligands had neutral interactions with the matrix BCP blocks, segregating the Au NPs to the PS/P2VP interface within the PS-*b*-P2VP film. However, exposure to UV light resulted in the photocleavage of the ester group in PNBA, converting it into hydrophilic PAA. Consequently, the NPs became uniformly distributed in the P2VP domain due to the hydrogen bonding between P2VP and PAA.

Another representative example can be found in the small molecule-directed approach, where small molecules serve as non-covalent linkers between BCPs and NP ligands. The assembly process is guided by the energetic cost arising from defects, the chain mobility, and the activation energy for inter-domain diffusion.[117] Their interactions can be modulated by external stimuli, either strengthened or weakened as needed. The Xu group exploited 3-*n*-pentadecylphenol (PDP) as a small molecule to create a supramolecular system with polystyrene-*block*-poly(4-vinyl pyridine) (PS-*b*-P4VP).[118] The hydrogen bonding between PDP and P4VP is weakened in response to

temperature above 100 °C. Strong hydrogen bonding induced the selective localization of CdSe NPs within the P4VP domain at low temperatures (*i.e.*, 50 °C). With increasing temperature to around 110 °C, PDP molecules became soluble in the PS domain, resulting in the segregation of the NPs at the PS/P4VP interface to minimize unfavorable interactions and entropic penalties. As the temperature was further increased to 150 °C, the breaking of the hydrogen bonds reduced the stiffness in the P4VP domain, decreasing the entropic driving force for the NPs to be located at the PS/P4VP interface. Consequently, a uniform distribution of NPs in the P4VP domain was achieved.

In contrast to the production of polymer films on a solid substrate, polymer composite films formed at a fluid interface offer higher mobility for both polymer chains and NPs, making it easier to achieve external field-induced assembly. The Park group reported the self-assembly of iron oxide NPs and conjugated BCPs, poly(3-hexyl thiophene)-*block*-poly(ethylene glycol) (P3HT-*b*-PEG), at the air/water interface under a magnetic field (Fig. 6(c)).[119] Due to the rod-coil configuration of P3HT-*b*-PEG, short polymer nanowires decorated with the NPs were created through the crystallization of P3HT followed by the growth of these magnetic subunits into macroscopically aligned nanowire arrays through the magnetic interaction. The NPs preferred to be located at the interface between P3HT and PEG due to the hydrophobic oleic acid on the NP surface and
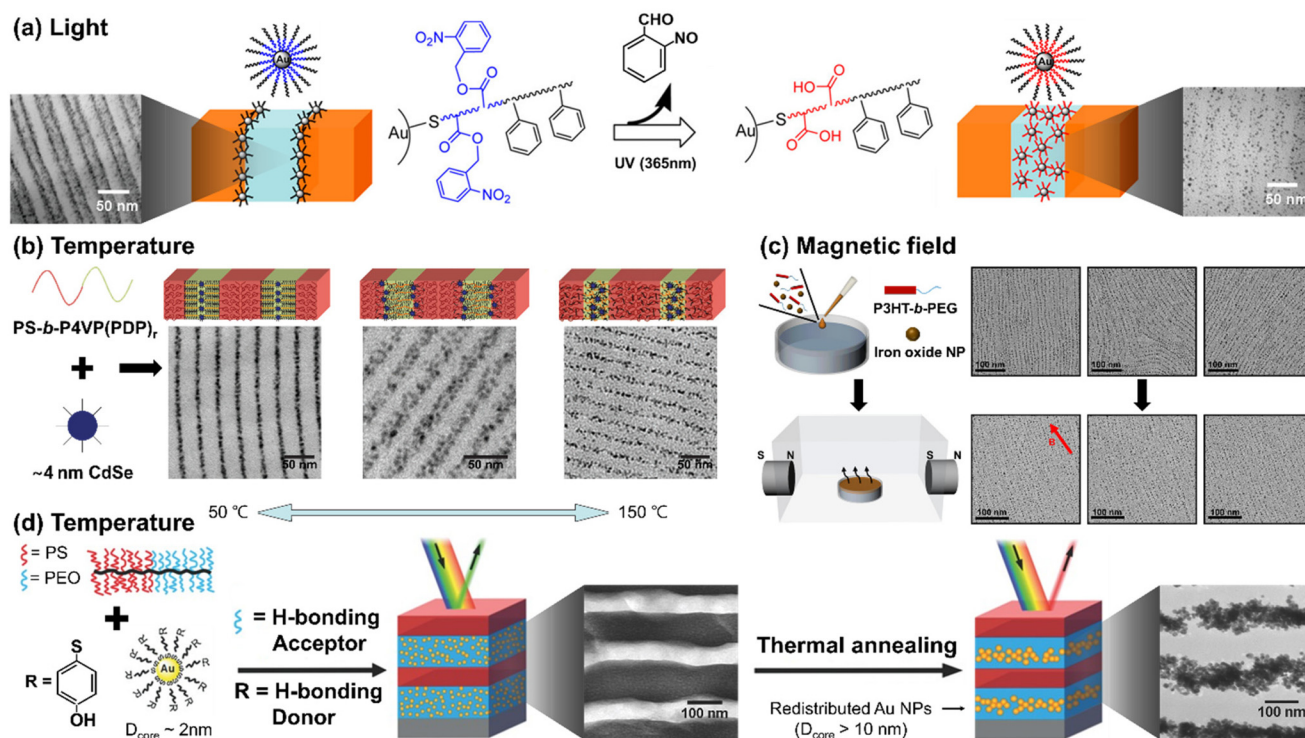

Fig. 6 Stimuli-responsive NP arrays within BCP matrices. (a) UV-responsive localization of core−shell Au NPs within the PS-*b*-P2VP. Reproduced from ref. 116 with permission from American Chemical Society 2014; (b) small-molecule-directed CdSe NP assembly in response to temperature. Reproduced from ref. 118 with permission from Nature Publishing Group 2009; (c) magnetic field-induced self-assembly of P3HT-*b*-PEG and iron oxide NPs at the air/water interface. Reproduced from ref. 119 with permission from American Chemical Society 2022; (d) thermally tunable Au NPs assembly in brush BCPs driven by the change of NPs size due to the ripening of NPs. Reproduced from ref. 122 with permission from Wiley 2015.

the strong crystallization of P3HTs. P3HT has a strong tendency to crystallize, which results in the expulsion of NPs out of the P3HT domain. As a result, these hydrophobic NPs tend to position themselves around polymer nanowires at the interface between P3HT and PEG to avoid contact with the water subphase. Under the magnetic field, the orientation of the array was aligned with the direction of the magnetic field. The key to achieving this lies in precise control of NP size, as the NPs should be neither too large to be affected by the entropy effect nor too small to enable effective magnetic dipole interactions.

While distinct from the principles underlying the enthalpy contributions discussed in this paper, it is worth noting that recent reports have demonstrated changes in NP assembly driven by stimuli-induced alterations in entropy contributions. For example, the Watkins group reported temperature-responsive growth of Au NPs capped with 4-mercaptophenol ligands. The Au NPs, which can grow at high temperatures due to thermally induced ripening,[120,121] were incorporated into brush block copolymers composed of poly(ethylene oxide) (PEO) and PS (Fig. 6(d)).[122] Initially, 2 nm Au NPs were selectively distributed in the PEO domain through hydrogen bonds between PEO and 4-mercaptophenol ligands on the Au surface. Upon annealing at 120 °C, however, their size increased to over 10 nm, resulting in the segregation of the NPs to the center of the PEO domain to reduce the entropy penalty associated with accommodating larger NPs.

3.3.3. Self-assembly of NPs at polymer/water interfaces.
The design principles governing the self-assembly of BCP/NP hybrid materials extend to three-dimensional systems. The controlled self-assembly of the BCPs within solvent-evaporative oil-in-water emulsions provides a robust and effective approach for creating polymer particles with precisely defined shapes, sizes, and internal nanostructures.[123–128] In these systems, emulsion droplets serve as flexible and dynamic templates that adaptively shape the polymer assembly as the solvent evaporates. This process yields a diverse array of polymer particles distinguished by intricate structures.[129–131] The selective interfacial interactions between the surrounding medium and each block of the BCPs dictate the orientation of the BCPs, ultimately determining the final particle shape.[132,133] In brief, when a neutral preference is provided for the BCPs and surrounding medium, all chains are exposed to their surroundings, leading to the formation of axially stacked lamellar structures for lamellar BCPs and hexagonally stacked cylinders for cylindrical BCPs. Due to their anisotropic symmetry, lamellar BCPs form prolate ellipsoids, while cylindrical BCPs adopt oblate lens shapes. Notably, NPs can induce such shape transformations by acting as surfactant,[24,134] in stark contrast to bulk and film systems. As demonstrated in the previous section, the location and distribution of NPs within the BCP particles are determined by the counterbalance of the enthalpic interaction between the NP and BCPs and the entropic penalty associated with BCP chain stretching to host NPs. More importantly, in a 3D emulsion system, the role of the interface between the BCP and the surrounding medium

becomes significant. When NPs are located at the interface between the BCP particle and the surrounding medium, they modulate the overall shape and inner morphology of the particles. In this section, we first introduce the fundamental principles for producing hybrid BCP/NP microparticles, with a particular focus on controlled NP assembly at the emulsion interface. We will then explore the stimuli-responsive NP assembly within 3D particles.

Self-assembly of NPs at the interface of the BCP microparticles and the surrounding medium was first reported by the Hawker group. As shown in Fig. 7(a), a crosslinked polymer shell was formed at the surface of Au NPs through the grafting of PS-b-PI. When these NPs were co-assembled with PS-b-P2VP during solvent evaporation, they were localized at the interface of the microparticles.[134] As a result, a remarkable change in shape and morphology from sphere to ellipsoid was achieved because the Au-based NPs could adsorb at the emulsion surface and highly affect the interfacial interactions between the BCPs and the surrounding media. In particular, the entropic contribution plays an important role in such NP surfactant systems, because the NPs should possess a preference for segregating to the particle surface rather than positioning within the BCP domain. At the same time, they must selectively favor interaction with the BCPs to prevent aggregation due to strong NP–NP interaction. In this context, a similar approach was also reported by the Kim group using a series of size-controlled Au NPs or length-controlled Cu Pt nanorods for PS-b-P4VP microparticles.[24,135] The small molecule linker, PDP was used to induce selective interaction of NPs with the P4VP block. Especially, the size- and length-dependent positioning of NPs in the BCP particles enabled the systematic modulation of the interfacial properties and induced the formation of anisotropic PS-b-P4VP particles such as prolate and oblate particles (Fig. 7(b)).[135] The ratio of the NP length to the size of the NP–hosting domain (i.e., P4VP(PDP)) was key to determining the segregation of the NPs within the PS-b-P4VP(PDP) particles, allowing morphological transitions within critical ranges.

The entropy-driven transition of particle morphologies was further investigated either by positioning surface-modified Au NPs at the PS/P4VP interface or inducing macrophase separation between polystyrene-block-poly(vinylpyridine) (PS-b-PVP) and Au NPs. Zhu and Jiang group reported Janus hybrid microparticles with a variety of shapes: ellipsoids with concentrated Au NPs at one pole, spheres with AuNPs enriched in a bulge on the surface, and more complex shapes like gourd-like, clover-like, and four-leaf-clover-like particles, which resulted from a hierarchical assembly of these Janus hybrid microparticles.[136,137] In these studies, adept regulation of enthalpy and entropy was achieved through strategic chemical modification of NP surface and careful control of NP size and volume fraction, efficiently guiding spatial arrangement and interaction at BCP interfaces. More recently, the Kim group reported unique BCP/NP hybrid particles with well-ordered hexagonal NP superlattices by introducing an important parameter known as the swelling ratio (Fig. 7(c)). This ratio is defined as the number-average molecular weight (M_n) of the
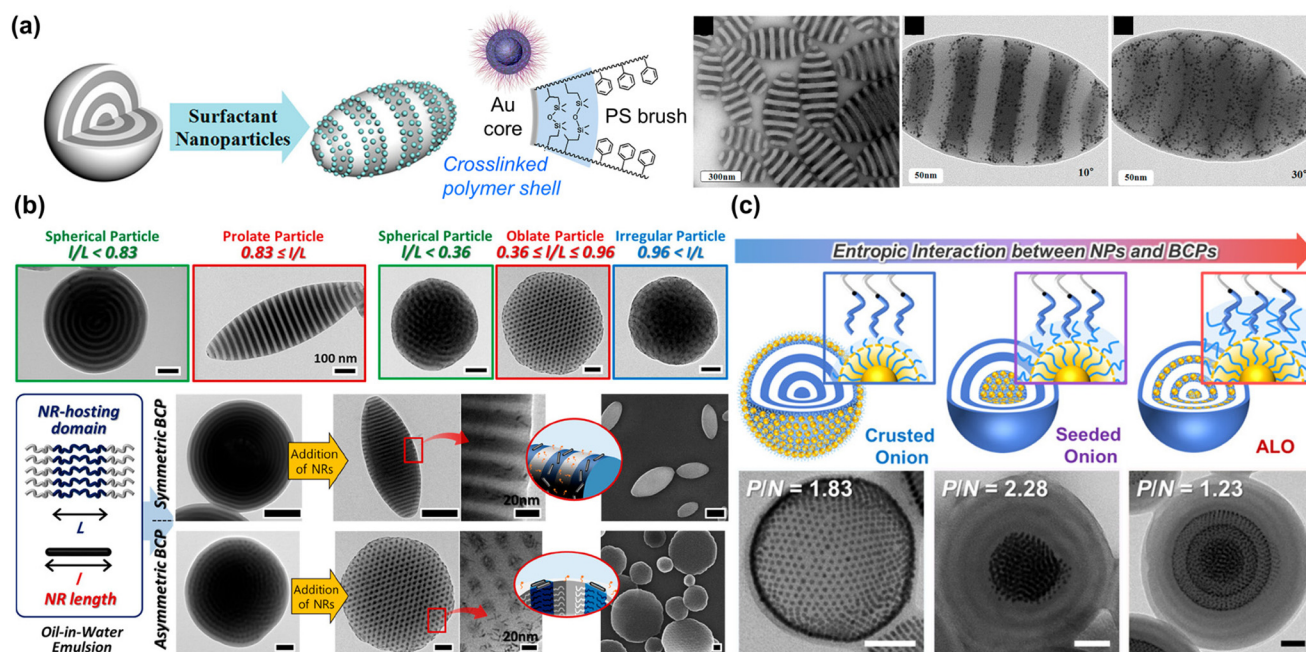
Fig. 7 Controlled assembly of BCPs and NPs within 3D microparticles to modulate overall particle shape or NP array. (a) Production of striped ellipsoids of PS-*b*-P2VP by using Au NPs as surfactants. Reproduced from ref. 134 with permission from American Chemical Society 2013; (b) shape transition of PS-*b*-P4VP particles driven by length-controlled CuPt nanorod surfactants. Reproduced from ref. 135 with permission from American Chemical Society 2018; (c) control of entropic interaction between PS-grafted Au NPs and PS-*b*-P4VP to form crusted onion, seeded onion, and alternated layered onion (ALO). Reproduced from ref. 139 with permission from American Chemical Society 2021.

polymer matrix relative to the M_n of the polymer ligand on the NP surface. Upon co-assembly of symmetric PS-*b*-P4VP and PS-coated Au NPs, Au NPs with low M_n ligands segregated either to the surface (*i.e.* crusted onion) or to the center (*i.e.*, seeded onion) of the spherical particles with radially stacked lamellae. In contrast, when Au NPs with higher M_n ligands were co-assembled with the same PS-*b*-P4VP, the NPs aligned at the center of the PS domains, forming alternate-layered, hexagonally packed superlattices within the spherical particles.[138] These phenomena were attributed to the autophobic dewetting behavior of NPs based on their swelling ratio with BCPs. With low M_n ligands, NPs were pushed to the surface or to the center due to the large entropic penalty on BCP domains. On the other hand, longer PS ligands could strongly interact with the PS chains of the BCPs, promoting the selective localization of the NPs with high M_n ligands in the PS domains. Further elaboration by systematic control of the Au NP diameter, grafting density, and M_n of the PS ligand was conducted to correlate morphological transitions of the hybrid particles to conformational changes of the PS ligands.[139]

To render these hybrid microparticles responsive to stimuli, dynamic positioning of NPs at the emulsion interface should be feasible, while maintaining the hydrophilic–lipophilic balance (HLB) required to form stable oil-in-water emulsions. However, once NPs are adsorbed on the particle surface, achieving reversibility becomes a challenge. Reversibility in polymer particles requires a solvent-mediated particle reconstruction process to provide sufficient mobility for the polymer

chains.[140,141] Only a limited number of examples of this process have been reported to date. Several examples involve the use of pH-responsive NPs with polystyrene-*block*-poly(dimethyl siloxane) (PS-*b*-PDMS) particles as the matrix. The Zhu group utilized iron oxide (Fe_3O_4) NPs coated with pH-responsive PAA-*b*-PS as co-surfactants for emulsions to modulate the shape of PS-*b*-PDMS particles (Fig. 8(a)). The addition of pH-responsive Fe_3O_4 NPs rendered the shape of pH-inert PS-*b*-PDMS microparticles sensitive to pH variations. This led to a change in the particle shape, transforming from an elongated Janus pupa-like structure to a bud-like and onion-like structure when the pH of the aqueous medium was increased.[142] At lower pH values, Janus pupa-like structures emerged, driven by the entropy penalty between the PS chains and NPs, resulting in NP aggregation at the end of the microparticles. With an increase in pH, the Fe_3O_4@PAA-*b*-PS NPs became amphiphilic, leading to the formation of a bud-like and an onion-like structure. Similar pH-responsive behavior was also observed in core-cross-linked PS-*b*-P4VP NPs.[143] As an example of structural changes in BCP particles in response to external stimuli, the Kim group demonstrated light-triggered shape changes in PS-*b*-P2VP particles by employing azobenzene-grafted Au NPs, whose ligands undergo photoisomerization as depicted in Fig. 8(b). Since the NPs were designed to be located at the BCP–water interface, the polarity of the NPs influenced the wetting layer on the BCP particle surface. When exposed to visible light, onion-like PS-*b*-P2VP particles with a PS outer layer formed, attributed to the nonpolar nature of
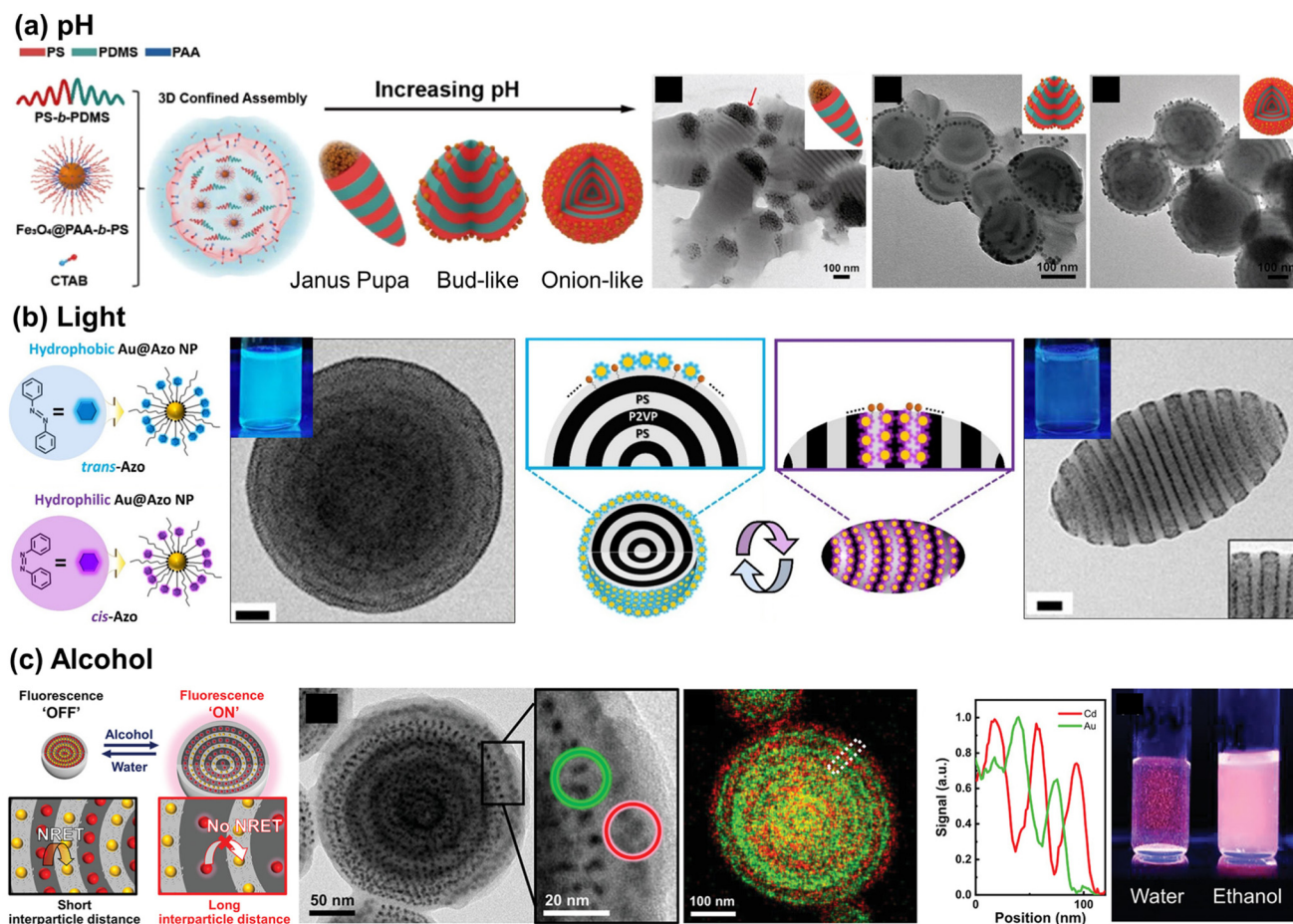
Fig. 8 Stimuli-responsive NP arrays within the polymer matrix. (a) pH-Responsive assembly of Fe$_3$O$_4$ NPs coated with PAA-*b*-PS within PS-*b*-PDMS particles. Reproduced from ref. 142 with permission from American Chemical Society 2021; (b) photo-switchable Au NP surfactants and their responsive assembly within BCP particles. Reproduced from ref. 144 with permission from American Chemical Society 2021; (c) solvent-responsive distance between QDs and Au NPs in doubly alternate-layered NP array and corresponding fluorescence switching behavior. Reproduced from ref. 145 with permission from Wiley 2021.

trans-Azo ligands on the NP surface. In contrast, UV-driven *trans*-to-*cis* isomerization of ligands shifted the polarity of NPs to be more hydrophilic, transforming these particles into ellipsoids with both PS and P2VP exposed on their surfaces.[144]

In addition to the examples of NPs acting as surfactants, another intriguing discovery involves utilizing a responsive BCP domain to exert precise control over the intermolecular NP distance in a reversible manner. This was achieved through the co-assembly of PS-grafted Au NPs (as quenchers) and CdSe/ZnS core/shell quantum dots (QDs, as emitters) within symmetric PS-*b*-P4VP particles. This process led to the creation of hybrid BCP particles with doubly alternating Au NP and QD layers due to the enthalpically favorable interaction with PS and P4VP domains, respectively, as depicted in Fig. 8(c).[145] When these hybrid particles were dispersed in water, the proximity of the Au NPs to the QD arrays resulted in quenching of the fluorescence of the QDs, due to strong nonradiative energy transfer from the QDs to Au NPs. Conversely, upon the addition of ethanol, the interparticle distance significantly increased due to the swelling of P4VP domains, effectively

inhibiting nonradiative energy transfer and thereby preserving the fluorescence of the particles. These examples highlight how structural changes in BCP particles, responsive to external stimuli, can be utilized to induce their functional property changes. This opens up significant possibilities for developing responsive smart colloidal materials.

4. Perspectives and conclusions

In this review, we have discussed the physical principles and recent strategic advances in the development of stimuli-responsive assembly of NPs at complex fluid interfaces. Current progress in creating responsive NP arrays at air/liquid, liquid/liquid, and polymer interfaces has primarily focused on experimental parameters to control dynamic packing structures and NP interactions. The key driving force to obtain a self-assembled NP array is the reduction in interfacial energy. On the nanoscale, particles face a balance between thermal fluctuations and interfacial energy, rendering self-assembly

size dependent. In designing a responsive NP assembly system, the ability to control the NP–NP interactions, NP–hosting fluid interaction, and their entropic contribution in response to stimuli is crucial. In the air/liquid interface systems, two primary strategies have been employed to address the entropy penalties associated with ordered arrays: (1) light- and temperature-induced structural transformations of functional groups, and (2) adjusting pH to control electrostatic repulsion. In the case of liquid/liquid interface systems, the surface charge of the NP ligands for electrostatic repulsion control can be tailored to respond to external stimuli such as pH, light, electric field, and heat. In the polymer/NP hybrid system, achieving reversible interfacial assembly relies on controlling the interaction between the NP and polymer interface, balancing between neutral selectivity and selective preference in response to stimuli. Novel approaches have emerged, including the introduction of small molecule linkers, grafting a mixture shell onto the NP core, and utilizing a controlled three-phase interaction (*i.e.*, water, polymer, and NP) for three-dimensional assembly.

Despite the numerous efforts to achieve stimuli-responsive NP assembly at complex fluid interfaces, several challenges should be addressed. First, NP assembly at the air/liquid interface often involves volatile liquids or surface tension gradients induced by solvent evaporation. To leverage external stimuli as a driving force, resolving issues like particle aggregation and the presence of voids in the array, as well as the generation of sufficient alteration in interfacial properties, requires a strategic design of inorganic core/organic shell structures. In addition, when employing polymers as NP ligands, the fluidity of the polymer chains limits the NP mobility, emphasizing the necessity for a polymer matrix design that allows faster NP movement. While a well-established thermodynamic theory addresses NP assemblies responsive to stimuli, a kinetic understanding is lacking, especially regarding the rate at which NPs assemble. Lastly, most of the research concerning NPs at the interface of two immiscible liquids has spotlighted dynamic transformations between stable Pickering emulsions and inverse structures. In addition, studies on the NPs at the air/liquid interface have focused on dynamic behaviors between ordered and disordered arrays. However, the design of responsive NP assembly across multiple interfaces remains unexplored. For example, starting at the liquid/liquid interface by forming a Pickering emulsion, it is conceivable to induce the migration of the NPs in the Pickering emulsion to the air/liquid interface with close-packed structures. Such multiple-phase transition becomes feasible with robust stimuli that detach the NPs from the liquid/liquid interface, ensuring efficient adsorption kinetics at the air/liquid interface. In the case of BCP systems, achieving responsive behavior has proven challenging, primarily due to difficulties in ensuring polymer chain mobility in the absence of a solvent. As a result, only a limited number of examples of polymer-mediated stimuli-responsive NP assembly have been developed to date. One potential avenue for achieving dynamic NP arrays in the absence of a solvent is the use of low T_g polymer or leveraging

pH-driven swelling/deswelling behavior in a polymer matrix. Photoacid, which can convert the light response into the chemical property, also can be utilized in the design of core/shell NP ligands, following a similar principle. From a broader materials science perspective, dynamic systems and networks comprising NPs and functional surface ligands represent an excellent starting point for designing and realizing dynamic assemblies that would perform programmed tasks such as sensing and spatiotemporal catalysis.

Author contributions

The manuscript was written using contributions of all authors. All authors have given approval to the final version of the manuscript.

Conflicts of interest

The authors declare no conflicts of interest.

Acknowledgements

References

1 A. Böker, J. He, T. Emrick and T. P. Russell, *Soft Matter*, 2007, **3**, 1231–1248.

2 S. Kinge, M. Crego-Calama and D. N. Reinhoudt, *ChemPhysChem*, 2008, **9**, 20–42.

3 L. Duan, C. Wang, W. Zhang, B. Ma, Y. Deng, W. Li and D. Zhao, *Chem. Rev.*, 2021, **121**, 14349–14429.

4 M. Grzelczak, J. Vermant, E. M. Furst and L. M. Liz-Marzán, *ACS Nano*, 2010, **4**, 3591–3605.

5 M. D. Scanlon, E. Smirnov, T. J. Stockmann and P. Peljo, *Chem. Rev.*, 2018, **118**, 3722–3751.

6 X. Li, L. Chen, Y. Ma, D. Weng, Z. Li, L. Song, X. Zhang, G. Yu and J. Wang, *Adv. Funct. Mater.*, 2022, **32**, 2205462.

7 Y. Lin, A. Böker, H. Skaff, D. Cookson, A. Dinsmore, T. Emrick and T. P. Russell, *Langmuir*, 2005, **21**, 191–194.

8 Z. Niu, J. He, T. P. Russell and Q. Wang, *Angew. Chem., Int. Ed.*, 2010, **49**, 10052–10066.

9 D. Liu, W. Cai, M. Marin, Y. Yin and Y. Li, *ChemNanoMat*, 2019, **5**, 1338–1360.

10 J. Forth, P. Y. Kim, G. Xie, X. Liu, B. A. Helms and T. P. Russell, *Adv. Mater.*, 2019, **31**, 1806370.

11 M. Z. Iqbal, I. Ali, W. S. Khan, X. Kong and E. Dempsey, *Mater. Des.*, 2021, **205**, 109694.

12 M. Grzelczak, L. M. Liz-Marzán and R. Klajn, *Chem. Soc. Rev.*, 2019, **48**, 1342–1361.

13 W. Lee, D. Kim, S. Lee, J. Park, S. Oh, G. Kim, J. Lim and J. Kim, *Nano Today*, 2018, **23**, 97–123.

14 S. Hou, L. Bai, D. Lu and H. Duan, *Acc. Chem. Res.*, 2023, **56**, 740–751.

15 S. Shi and T. P. Russell, *Adv. Mater.*, 2018, **30**, 1800714.

16 S. K. Ghosh and A. Böker, *Macromol. Chem. Phys.*, 2019, **220**, 1900196.

17 J. Owen, *Science*, 2015, **347**, 615–616.

18 J. J. Giner-Casares and J. Reguera, *Nanoscale*, 2016, **8**, 16589–16595.

19 A. J. Zarbin, *Mater. Horiz.*, 2021, **8**, 1409–1432.

20 R. Dong, T. Zhang and X. Feng, *Chem. Rev.*, 2018, **118**, 6189–6235.

21 F. Bresme and M. Oettel, *J. Phys.: Condens. Matter*, 2007, **19**, 413101.

22 L. Hu, M. Chen, X. Fang and L. Wu, *Chem. Soc. Rev.*, 2012, **41**, 1350–1362.

23 B. P. Binks, *Curr. Opin. Colloid Interface Sci.*, 2002, **7**, 21–41.

24 K. H. Ku, J. M. Shin, M. P. Kim, C.-H. Lee, M.-K. Seo, G.-R. Yi, S. G. Jang and B. J. Kim, *J. Am. Chem. Soc.*, 2014, **136**, 9982–9989.

25 K. H. Ku, J. M. Shin, H. Yun, G. R. Yi, S. G. Jang and B. J. Kim, *Adv. Funct. Mater.*, 2018, **28**, 1802961.

26 L. Xu, G. Han, J. Hu, Y. He, J. Pan, Y. Li and J. Xiang, *Phys. Chem. Chem. Phys.*, 2009, **11**, 6490–6497.

27 O. S. Deshmukh, D. van den Ende, M. C. Stuart, F. Mugele and M. H. Duits, *Adv. Colloid Interface Sci.*, 2015, **222**, 215–227.

28 J. Vialetto and M. Anyfantakis, *Langmuir*, 2021, **37**, 9302–9335.

29 V. Sashuk, K. Winkler, A. Zywocinski, T. Wojciechowski, E. Gorecka and M. Fiałkowski, *ACS Nano*, 2013, **7**, 8833–8839.

30 V. Garbin, J. C. Crocker and K. J. Stebe, *J. Colloid Interface Sci.*, 2012, **387**, 1–11.

31 X. Lu, Y. Huang, B. Liu, L. Zhang, L. Song, J. Zhang, A. Zhang and T. Chen, *Chem. Mater.*, 2018, **30**, 1989–1997.

32 R. Zbonikowski, M. Iwan and J. Paczesny, *ACS Omega*, 2023, **8**, 23706–23719.

33 M. Zhang, Z. Hou, H. Wang, L. Zhang, J. Xu and J. Zhu, *Langmuir*, 2020, **37**, 454–460.

34 J. K. Stolarczyk, A. Deak and D. F. Brougham, *Adv. Mater.*, 2016, **28**, 5400–5424.

35 G. Zhu, Z. Huang, Z. Xu and L.-T. Yan, *Acc. Chem. Res.*, 2018, **51**, 900–909.

36 C. Huang, X. Chen, Z. Xue and T. Wang, *Acc. Chem. Res.*, 2020, **54**, 35–45.

37 S. J. Kim, J. Choi, K. Maleski, K. Hantanasirisakul, H.-T. Jung, Y. Gogotsi and C. W. Ahn, *ACS Appl. Mater. Interfaces*, 2019, **11**, 32320–32327.

38 S. Kutuzov, J. He, R. Tangirala, T. Emrick, T. Russell and A. Böker, *Phys. Chem. Chem. Phys.*, 2007, **9**, 6351–6358.

39 D. A. Walker, B. Kowalczyk, M. O. de La Cruz and B. A. Grzybowski, *Nanoscale*, 2011, **3**, 1316–1344.

40 J. N. Israelachvili, *Contemp. Phys.*, 1974, **15**, 159–178.

41 M. Liu, M. Yang, X. Wan, Z. Tang, L. Jiang and S. Wang, *Adv. Mater.*, 2023, **35**, 2208995.

42 D. Wang, B. Kowalczyk, I. Lagzi and B. A. Grzybowski, *J. Phys. Chem.*, 2010, **1**, 1459–1462.

43 X. Li, X. Liu and X. Liu, *Chem. Soc. Rev.*, 2021, **50**, 2074–2101.

44 G. Pasparakis, T. Manouras, P. Argitis and M. Vamvakaki, *Macromol. Rapid Commun.*, 2012, **33**, 183–198.

45 X. Yao, T. Li, J. Wang, X. Ma and H. Tian, *Adv. Opt. Mater.*, 2016, **4**, 1322–1349.

46 R. Klajn, K. J. Bishop, M. Fialkowski, M. Paszewski, C. J. Campbell, T. P. Gray and B. A. Grzybowski, *Science*, 2007, **316**, 261–264.

47 H. Zhang and D. Wang, *Angew. Chem.*, 2008, **120**, 4048–4051.

48 R. Klajn, K. J. Bishop and B. A. Grzybowski, *Proc. Natl. Acad. Sci. U. S. A.*, 2007, **104**, 10305–10309.

49 E. Blasco, M. Wegener and C. Barner-Kowollik, *Adv. Mater.*, 2017, **29**, 1604005.

50 J. Zhang, P. J. Santos, P. A. Gabrys, S. Lee, C. Liu and R. J. Macfarlane, *J. Am. Chem. Soc.*, 2016, **138**, 16228–16231.

51 W. Blokzijl and J. B. Engberts, *Angew. Chem., Int. Ed. Engl.*, 1993, **32**, 1545–1579.

52 Y. Sahoo, M. Cheon, S. Wang, H. Luo, E. Furlani and P. Prasad, *J. Phys. Chem. B*, 2004, **108**, 3380–3383.

53 D. Liu, C. Li, F. Zhou, T. Zhang, G. Liu, W. Cai and Y. Li, *Adv. Mater. Interfaces*, 2017, **4**, 1600976.

54 T. Zhao, P. Xie, H. Wan, T. Ding, M. Liu, J. Xie, E. Li, X. Chen, T. Wang and Q. Zhang, *Nat. Photonics*, 2023, **17**, 622–628.

55 B. Kim, S. L. Tripp and A. Wei, *J. Am. Chem. Soc.*, 2001, **123**, 7955–7956.

56 N. J. Brewer, R. E. Rawsterne, S. Kothari and G. J. Leggett, *J. Am. Chem. Soc.*, 2001, **123**, 4089–4090.

57 T. Nishimura, N. Ito, K. Kinoshita, M. Matsukawa, Y. Imura and T. Kawai, *Small*, 2020, **16**, 1903365.

58 F. Nakagawa, R. Kichijo, M. Matsukawa, K.-H. Wang, Y. Imura and T. Kawai, *Colloids Surf., A*, 2023, **656**, 130499.

59 X. Liu, M. Atwater, J. Wang, Q. Dai, J. Zou, J. P. Brennan and Q. Huo, *J. Nanosci. Nanotechnol.*, 2007, **7**, 3126–3133.

60 F. Zheng, Y. Zhang, L. Dong, D. Zhao, R. Feng, P. Tao, W. Shang, B. Fu, C. Song and T. Deng, *Nanoscale*, 2021, **13**, 20521–20530.

61 S. Roy, R. K. Kashyap and P. P. Pillai, *J. Phys. Chem. C*, 2023, **127**, 10355–10365.

62 H. Zhang, S. Nayak, W. Wang, S. Mallapragada and D. Vaknin, *Langmuir*, 2017, **33**, 12227–12234.

63 F. Reincke, S. G. Hickey, W. K. Kegel and D. Vanmaekelbergh, *Angew. Chem., Int. Ed.*, 2004, **43**, 458–462.

64 B. Liu, X. Lu, Z. Qiao, L. Song, Q. Cheng, J. Zhang, A. Zhang, Y. Huang and T. Chen, *Langmuir*, 2018, **34**, 13047–13056.

65 K. H. Ku, J. Li, K. Yoshinaga and T. M. Swager, *Adv. Mater.*, 2019, **31**, 1905569.

66 A. Dinsmore, M. F. Hsu, M. Nikolaides, M. Marquez, A. Bausch and D. Weitz, *Science*, 2002, **298**, 1006–1009.

67 J. Wu and G. H. Ma, *Small*, 2016, **12**, 4633–4648.

68 H. Jiang, Y. Sheng and T. Ngai, *Curr. Opin. Colloid Interface Sci.*, 2020, **49**, 1–15.

69 R. Aveyard, B. P. Binks and J. H. Clint, *Adv. Colloid Interface Sci.*, 2003, **100**, 503–546.

70 H. Sun, L. Li, T. P. Russell and S. Shi, *J. Am. Chem. Soc.*, 2020, **142**, 8591–8595.

71 H. Sun, M. Li, L. Li, T. Liu, Y. Luo, T. P. Russell and S. Shi, *J. Am. Chem. Soc.*, 2021, **143**, 3719–3722.

72 K. Watanabe, T. A. Welling, S. Sadighikia, H. Ishii, A. Imhof, M. A. van Huis, A. van Blaaderen and D. Nagao, *J. Colloid Interface Sci.*, 2020, **566**, 202–210.

73 M. K. Bera, H. Chan, D. F. Moyano, H. Yu, S. Tatur, D. Amoanu, W. Bu, V. M. Rotello, M. Meron and P. Král, *Nano Lett.*, 2014, **14**, 6816–6822.

74 Y. Montelongo, D. Sikdar, Y. Ma, A. J. McIntosh, L. Velleman, A. R. Kucernak, J. B. Edel and A. A. Kornyshev, *Nat. Mater.*, 2017, **16**, 1127–1135.

75 M. N. Martin, J. I. Basham, P. Chando and S.-K. Eah, *Langmuir*, 2010, **26**, 7410–7417.

76 M. J. Junk, W. Li, A. D. Schlüter, G. Wegner, H. W. Spiess, A. Zhang and D. Hinderberger, *J. Am. Chem. Soc.*, 2011, **133**, 10832–10838.

77 H. Tian, H. Li and Y. Fang, *ACS Appl. Mater. Interfaces*, 2019, **11**, 16207–16213.

78 L. Song, B. B. Xu, Q. Cheng, X. Wang, X. Luo, X. Chen, T. Chen and Y. Huang, *Sci. Adv.*, 2021, **7**, eabk2852.

79 Y.-K. Park and S. Park, *Chem. Mater.*, 2008, **20**, 2388–2393.

80 Z. Li, Y. Shi, A. Zhu, Y. Zhao, H. Wang, B. P. Binks and J. Wang, *Angew. Chem.*, 2021, **133**, 3974–3979.

81 S. Acter, M. L. P. Vidallon, J. P. King, B. M. Teo and R. F. Tabor, *J. Mater. Chem. B*, 2021, **9**, 8962–8970.

82 L. Zhang, G. Zhang, J. Ge, P. Jiang and L. Ding, *J. Colloid Interface Sci.*, 2022, **616**, 129–140.

83 S. Björkegren, M. C. A. Freixiela Dias, K. Lundahl, L. Nordstierna and A. Palmqvist, *Langmuir*, 2020, **36**, 2357–2367.

84 S. Yu, M. Lv, G. Lu, C. Cai, J. Jiang and Z. Cui, *Langmuir*, 2021, **37**, 10683–10691.

85 K. Liu, J. Jiang, Z. Cui and B. P. Binks, *Langmuir*, 2017, **33**, 2296–2305.

86 Y. Zhang, X. Ren, S. Guo, X. Liu and Y. Fang, *ACS Sustainable Chem. Eng.*, 2018, **6**, 2641–2650.

87 Y. Shi, D. Xiong, Y. Chen, H. Wang and J. Wang, *J. Mol. Liq.*, 2019, **274**, 239–245.

88 H. Li, Y. Liu and J. Jiang, *Green Chem.*, 2022, **24**, 8062–8068.

89 S. Yu, D. Zhang, J. Jiang, Z. Cui, W. Xia, B. P. Binks and H. Yang, *Green Chem.*, 2019, **21**, 4062–4068.

90 A. Alvarez-Fernandez, C. Cummins, M. Saba, U. Steiner, G. Fleury, V. Ponsinet and S. Guldin, *Adv. Opt. Mater.*, 2021, **9**, 2100175.

91 A. C. Balazs, T. Emrick and T. P. Russell, *Science*, 2006, **314**, 1107–1110.

92 C. Yi, Y. Yang, B. Liu, J. He and Z. Nie, *Chem. Soc. Rev.*, 2020, **49**, 465–508.

93 L. Zhai, *Chem. Soc. Rev.*, 2013, **42**, 7148–7160.

94 C. Xu, B. B. Wayland, M. Fryd, K. I. Winey and R. J. Composto, *Macromolecules*, 2006, **39**, 6063–6070.

95 I. Tokarev and S. Minko, *Adv. Mater.*, 2009, **21**, 241–247.

96 J. Wang, W. Li and J. Zhu, *Polymer*, 2014, **55**, 1079–1096.

97 J. Kao, K. Thorkelsson, P. Bai, B. J. Rancatore and T. Xu, *Chem. Soc. Rev.*, 2013, **42**, 2654–2678.

98 W. A. Lopes and H. M. Jaeger, *Nature*, 2001, **414**, 735–738.

99 J. Huang, A. Hall, I. Jayapurna, S. Algharbi, V. Ginzburg and T. Xu, *Macromolecules*, 2021, **54**, 1006–1016.

100 K. H. Ku, H. Yang, S. G. Jang, J. Bang and B. J. Kim, *J. Polym. Sci., Part A: Polym. Chem.*, 2016, **54**, 228–237.

101 B. Sarkar and P. Alexandridis, *Prog. Polym. Sci.*, 2015, **40**, 33–62.

102 Y. Gai, Y. Lin, D.-P. Song, B. M. Yavitt and J. J. Watkins, *Macromolecules*, 2016, **49**, 3352–3360.

103 S.-W. Hsu and T. Xu, *Macromolecules*, 2019, **52**, 2833–2842.

104 M. Konefał, P. Černoch, V. Patsula, E. Pavlova, J. Dybal, K. Załęski and A. Zhigunov, *ACS Appl. Mater. Interfaces*, 2021, **13**, 9195–9205.

105 D.-P. Song, C. Li, W. Li and J. J. Watkins, *ACS Nano*, 2016, **10**, 1216–1223.

106 D.-P. Song, S. Shahin, W. Xie, S. Mehravar, X. Liu, C. Li, R. A. Norwood, J.-H. Lee and J. J. Watkins, *Macromolecules*, 2016, **49**, 5068–5075.

107 L. Yao, Y. Lin and J. J. Watkins, *Macromolecules*, 2014, **47**, 1844–1849.

108 J. Kao, P. Bai, J. M. Lucas, A. P. Alivisatos and T. Xu, *J. Am. Chem. Soc.*, 2013, **135**, 1680–1683.

109 K. C. Bryson, T. I. Löbling, A. H. E. Müller, T. P. Russell and R. C. Hayward, *Macromolecules*, 2015, **48**, 4220–4227.

110 S. Kim, M. Yoo, N. Kang, B. Moon, B. J. Kim, S.-H. Choi, J. U. Kim and J. Bang, *ACS Appl. Mater. Interfaces*, 2013, **5**, 5659–5666.

111 B. J. Kim, J. Bang, C. J. Hawker, J. J. Chiu, D. J. Pine, S. G. Jang, S.-M. Yang and E. J. Kramer, *Langmuir*, 2007, **23**, 12693–12703.

112 B. J. Kim, J. Bang, C. J. Hawker and E. J. Kramer, *Macromolecules*, 2006, **39**, 4108–4114.

113 S. G. Jang, E. J. Kramer and C. J. Hawker, *J. Am. Chem. Soc.*, 2011, **133**, 16986–16996.

114 S. G. Jang, A. Khan, M. D. Dimitriou, B. J. Kim, N. A. Lynd, E. J. Kramer and C. J. Hawker, *Soft Matter*, 2011, **7**, 6255–6263.

115 S. G. Jang, B. J. Kim, C. J. Hawker and E. J. Kramer, *Macromolecules*, 2011, **44**, 9366–9373.

116 D.-P. Song, X. Wang, Y. Lin and J. J. Watkins, *J. Phys. Chem. B*, 2014, **118**, 12788–12795.

117 J. Kao, K. Thorkelsson, P. Bai, Z. Zhang, C. Sun and T. Xu, *Nat. Commun.*, 2014, **5**, 4053.

118 Y. Zhao, K. Thorkelsson, A. J. Mastroianni, T. Schilling, J. M. Luther, B. J. Rancatore, K. Matsunaga, H. Jinnai,

Y. Wu, D. Poulsen, J. M. J. Fréchet, A. Paul Alivisatos and T. Xu, *Nat. Mater.*, 2009, **8**, 979–985.

119 M. Park, S. Kang, C. Nam, K. Narasimha, W. B. Lee and S.-J. Park, *ACS Appl. Mater. Interfaces*, 2022, **14**, 8266–8273.

120 N. G. Bastús, J. Comenge and V. Puntes, *Langmuir*, 2011, **27**, 11098–11105.

121 T. Shimizu, T. Teranishi, S. Hasegawa and M. Miyake, *J. Phys. Chem. B*, 2003, **107**, 2719–2724.

122 D.-P. Song, C. Li, N. S. Colella, X. Lu, J.-H. Lee and J. J. Watkins, *Adv. Opt. Mater.*, 2015, **3**, 1169–1175.

123 D. Hu, Y. Wang, J. Liu, Y. Mao, X. Chang and Y. Zhu, *Nanoscale*, 2022, **14**, 6291–6298.

124 S.-J. Jeon, S.-M. Yang, B. J. Kim, J. D. Petrie, S. G. Jang, E. J. Kramer, D. J. Pine and G.-R. Yi, *Chem. Mater.*, 2009, **21**, 3739–3741.

125 K. H. Ku, J. M. Shin, H. Yun, G.-R. Yi, S. G. Jang and B. J. Kim, *Adv. Funct. Mater.*, 2018, **28**, 1802961.

126 J. M. Shin, Y. Kim, H. Yun, G.-R. Yi and B. J. Kim, *ACS Nano*, 2017, **11**, 2133–2142.

127 C. K. Wong, X. Qiang, A. H. E. Müller and A. H. Gröschel, *Prog. Polym. Sci.*, 2020, **102**, 101211.

128 N. Yan, Y. Zhu and W. Jiang, *Chem. Commun.*, 2018, **54**, 13183–13195.

129 J. Kim, H. Yun, Y. J. Lee, J. Lee, S.-H. Kim, K. H. Ku and B. J. Kim, *J. Am. Chem. Soc.*, 2021, **143**, 13333–13341.

130 K. H. Ku, M. P. Kim, K. Paek, J. M. Shin, S. Chung, S. G. Jang, W.-S. Chae, G.-R. Yi and B. J. Kim, *Small*, 2013, **9**, 2667–2672.

131 K. H. Ku, J. M. Shin, D. Klinger, S. G. Jang, R. C. Hayward, C. J. Hawker and B. J. Kim, *ACS Nano*, 2016, **10**, 5243–5251.

132 D. Klinger, C. X. Wang, L. A. Connal, D. J. Audus, S. G. Jang, S. Kraemer, K. L. Killops, G. H. Fredrickson, E. J. Kramer and C. J. Hawker, *Angew. Chem., Int. Ed.*, 2014, **53**, 7018–7022.

133 K. H. Ku, Y. J. Lee, Y. Kim and B. J. Kim, *Macromolecules*, 2019, **52**, 1150–1157.

134 S. G. Jang, D. J. Audus, D. Klinger, D. V. Krogstad, B. J. Kim, A. Cameron, S.-W. Kim, K. T. Delaney, S.-M. Hur, K. L. Killops, G. H. Fredrickson, E. J. Kramer and C. J. Hawker, *J. Am. Chem. Soc.*, 2013, **135**, 6649–6657.

135 K. H. Ku, J. H. Ryu, J. Kim, H. Yun, C. Nam, J. M. Shin, Y. Kim, S. G. Jang, W. B. Lee and B. J. Kim, *Chem. Mater.*, 2018, **30**, 8669–8678.

136 N. Yan, H. Liu, Y. Zhu, W. Jiang and Z. Dong, *Macromolecules*, 2015, **48**, 5980–5987.

137 N. Yan, Y. Zhang, Y. He, Y. Zhu and W. Jiang, *Macromolecules*, 2017, **50**, 6771–6778.

138 M. Xu, K. H. Ku, Y. J. Lee, J. J. Shin, E. J. Kim, S. G. Jang, H. Yun and B. J. Kim, *Chem. Mater.*, 2020, **32**, 7036–7043.

139 M. Xu, K. H. Ku, Y. J. Lee, T. Kim, J. J. Shin, E. J. Kim, S.-H. Choi, H. Yun and B. J. Kim, *Macromolecules*, 2021, **54**, 3084–3092.

140 J. M. Shin, Y. J. Lee, M. Kim, K. H. Ku, J. Lee, Y. Kim, H. Yun, K. Liao, C. J. Hawker and B. J. Kim, *Chem. Mater.*, 2019, **31**, 1066–1074.

141 R. Deng, F. Liang, W. Li, Z. Yang and J. Zhu, *Macromolecules*, 2013, **46**, 7012–7017.

142 Z. Hou, M. Ren, K. Wang, Y. Yang, J. Xu and J. Zhu, *Macromolecules*, 2020, **53**, 473–481.

143 M. Zhang, Z. Hou, H. Wang, L. Zhang, J. Xu and J. Zhu, *Langmuir*, 2021, **37**, 454–460.

144 S. H. Kwon, M. Xu, J. Kim, E. J. Kim, Y. J. Lee, S. G. Jang, H. Yun and B. J. Kim, *Chem. Mater.*, 2021, **33**, 9769–9779.

145 T. Kim, M. Xu, Y. J. Lee, K. H. Ku, D. J. Shin, D. C. Lee, S. G. Jang, H. Yun and B. J. Kim, *Small*, 2021, **17**, 2101222.